Engineering with Computers (2022) 38:1465–1490
https://doi.org/10.1007/s00366-020-01107-7

ORIGINAL ARTICLE

A finite element formulation using four-unknown incorporating nonlocal theory for bending and free vibration analysis of functionally graded nanoplates resting on elastic medium foundations

Van-Ke Tran[1] · Quoc-Hoa Pham[2,3] · Trung Nguyen-Thoi[2,3]

Received: 16 November 2019 / Accepted: 7 July 2020 / Published online: 24 July 2020

Abstract
A finite element model using four-unknown shear deformation theory integrated with the nonlocal theory is proposed for the bending and free vibration analysis of functionally graded (FG) nanoplates resting on elastic foundations. The present study developed the four-node quadrilateral element using Lagrangian and Hermitian interpolation functions for analysis of the membrane and bending displacement fields of FG nanoplates. Such a finite element formulation is suitable to investigate for the FG nanoplates resting on the elastic medium foundation with the stiffness matrices, the mass matrices and the load vectors using the second derivatives. The material properties of FG nanoplates are assumed to vary through the thickness direction by a power rule distribution of volume-fractions of the constituents. The equation of motion for FG nanoplates resting on the elastic foundation is obtained through Hamilton's principle. Several numerical results are presented to demonstrate the accuracy and reliability of the present approach in comparison with other existing methods. In addition, the effects of geometrical parameters, material parameters, nonlocal parameters on the static bending and the free vibration responses of the nanoplates is also investigated in detail.

Keywords Nonlocal elasticity · FG material · Elastic foundation · Four-unknown shear deformation theory · FEM

1 Introduction

Due to superior mechanical, chemical, thermal and electronic properties, in recent years, nanostructures have been widely interested by many scientists in the micro-electro-mechanical system (MEMs) and nano-electro-mechanical system (NEMs). However, nano experiments and molecular dynamics (MD) simulation is not only difficult but also very expensive, and hence the development of mathematical models in evaluating the mechanical behavior of structures at the nanoscale becomes an urgent problem. In the literature, there are three general types of mathematical models to perform the analysis of nanostructures including atomistic [1], hybrid atomistic continuum mechanics [2] and continuum mechanics. For continuum mechanics, the nonlocal elasticity theory [3, 4], which considers small-scale effects with good accuracy and satisfactory agreements with molecular dynamics has been used. In this theory, the stress at one point is assumed as a function of the strain field at its neighboring. Besides, the inter-atomic forces and the atomic size scales, called the nonlocal parameters, are incorporated into constitutive equations in a nonlocal theory. This nonlocal model showed a good agreement with MD simulations and experiments for free vibration of the nanoplate problems [5–8], and was extensively applied to investigate the various performances of nanoplates [9–21].

Recently, the application of FG materials has been widely spread in nanoscale devices such as thin films [22, 23], and NEMS [24] due to their excellent performance. It is well known that FG materials are the advanced engineering composite materials with continuous variation of material properties from one surface to the other through the thickness and thus eliminate the concentration stress found in

✉ Quoc-Hoa Pham
phamquochoa@tdtu.edu.vn

1 Faculty of Mechanical Engineering, Le Qui Don University, Hanoi, Vietnam

2 Division of Computational Mathematics and Engineering, Institute for Computational Science, Ton Duc Thang University, Ho Chi Minh City, Vietnam

3 Faculty of Civil Engineering, Ton Duc Thang University, Ho Chi Minh City, Vietnam

laminated composites. Many works have been proposed for the bending, free vibration and buckling analyses of the FG nanoplates considering the small-scale effects. For example, Natarajan et al. [25] investigated the free flexural vibration of FG nanoplates with power-law distribution model and computed the effective properties by the Mori–Tanaka homogenization scheme. Jung and Han [26] studied bending and vibration responses of the Sigmoid FGM nanoplates using the Navier's solution. Nami et al. [27] analyzed the thermal buckling of the FG rectangular nanoplates with assuming the material properties of FG nanoplates according to the power-law distribution. In this study, the authors used the third-order shear deformation plate theory including nonlocal elasticity to build the governing equations of the nanoplates. Hashemi et al. [28] studied the free vibration of FG circular/annular plates with moderately thick based on the Mindlin plate theory and considered a small-scale effect on natural frequencies. Salehipour et al. [29] established the exact analytical solution of the free vibration of FG micro/nanoplates by the three-dimensional theory of elasticity accounting small-scale effect. Salehipour et al. [30] developed the modified nonlocal elasticity for the examination of the natural frequency of the FG micro/nanoplates. Ansari et al. [31] analyzed the bending and vibration of FG nanoplates with three-dimensional plate theory in conjunction with Eringen's nonlocal theory. In addition, the use of surface effects or the nonlocal plate theories to investigate for nanostructure behaviors has been conducted in many works. For instance, Karimi et al. [32] combined surface effects and nonlocal refined plate theories to analyze the buckling and vibration of the silver nanoplates. Karimi and Shahidi [33, 34] used the theories of the nonlocal, refined plate, and surface effects to investigate the free vibration response of square and skew magneto-electro-elastic nanoplates resting on elastic foundations. Also, using the Galerkin and Navier's method to investigate the magnitudes of surface energy stress in synchronous and asynchronous bending/buckling analysis of slanting double-layer was introduced in Ref. [35, 36]. Farajpour et al. [37] developed the Brinson model, nonlocal elasticity and Pasternak foundation model to study the effect of biaxial preload on the vibrational behavior of small-scale composite sheets reinforced by shape memory alloy nanofibers. Karami et al. [38] used the generalized differential quadrature method and nonlocal elasticity theory to examine positive and negative surface effects on the buckling and vibration of nanoplates subjected to biaxial and shear in-plane loadings. In addition, the use of the finite difference method based on surface effects combining with nonlocal elasticity theories was proposed to analyze nanostructures in Refs.[39–42]. Farajpour et al. [43] proposed an integral form of nonlocal elasticity with two distinct phases to investigate wave propagations in carbon nanotubes conveying nanofluid under the magneto-hygro-mechanical loading. Karimi and Rafieian [44] based on the nonlocal strain gradient and modified couple stress models to investigate the free vibration of BiTiO3–CoFe2O4 nanoplates.

Recently, the nanostructures such as graphene sheets have also been founded to be embedded in various mediums (such as polymer composites) with the aim of enhancing the strength of parent material. To date, some studies have been performed to model the mechanical behaviors of nanostructures embedded in elastic mediums. For example, Wang and Li [45] studied the bending behavior of the nanoplates embedded in an elastic matrix. Narendar and Gopalakrishnan [46] investigated the wave dispersion of a single-layered graphene sheet embedded in an elastic polymer matrix at Terahertz frequency level. Pouresmaeeli et al. [47] examined the vibration of viscoelastic orthotropic nanoplates embedded in a viscoelastic medium. Zenkour and Sobhy [48] investigated thermal buckling of nanoplates resting on the Winkler-Pasternak elastic medium, based on the sinusoidal shear deformation plate theory. Panyatong et al. [49] investigated the bending behavior of nanoplates embedded in an elastic medium including nonlocal elasticity and surface stress. In the above-mentioned works, most of them used analytical solutions to investigate the behavior of FG nanoplates resting on the elastic foundation. However, the analytical solutions are limited or even impossible when the geometry, boundary conditions and types of the load become more complicated. As an alternative, numerical methods have been proposed to overcome the limits of of these problems.

In the other front of developing the numerical methods for plate structures, Shimpi [50] proposed a displacement field with the separation of the bending and shear components to improve the first-order shear deformation theory (FSDT). The most interesting points of this theory are the use of fewer unknowns in the governing equations than the original FSDT and have no requirement of any shear correction factor. Some researchers developed the four-unknown shear deformation theories for the analysis of various problems. Specifically, Mechab et al. [51].conducted the static analysis of the functionally graded plates using the refined plate theory with four unknowns. In this study, the Navier method was used to build the governing equation for the FG plates under the sinusoidal distributed load. Benachour et al. [52] extended the four-unknown refined plate theory and the Navier method to derive the governing equation for free vibration analysis of the FG plates. Thai et al. [53] presented the finite element method using the four-unknown shear deformation theories to study the bending and free vibration analysis for FG plates. Based on the four-unknown shear deformation theories and the nonlocal theory, Sobhy [54] studied the static, free vibration and buckling response of the FG nanoplates resting on the elastic foundation. To the best of authors' knowledge, most of above-mentioned works only focus on using the finite element method combining the four-unknown shear deformation theories to study for macrostructures, and there have been very few articles using numerical methods for the analysis of FG nanoplates. It hence motivates us to develop a finite element method using the four-unknown shear deformation theory for analysis of the FGP nanoplates.

To fill in the above-mentioned research gaps, this article is performed to develop a finite element method using the four-unknown shear deformation theory and nonlocal theory to accurately describe the stress and the displacement field of the FG nanoplates resting on the elastic foundation. Due to using the techniques of a numerical method, the proposed method will be very suitable to analyze for the complex nanostructures with arbitrary boundary and load conditions. The accuracy and reliability of the proposed method will be demonstrated by comparing the present numerical results with those of published works. Furthermore, the influence of geometrical parameters, material parameters, elastic foundation parameters to the static bending and the free vibrations of the FG nanoplates are also examined. The paper is organized as follows: A brief review of materials and works dealing with this problem is introduced in Sect. 1. Theoretical formulations are presented in Sect. 2. Verification examples, numerical results, and discussions are performed in Sect. 3. Section 4 concludes some highlight results and new contributions of this work.

2 Theoretical formulation

2.1 FG nanoplates resting on elastic foundations

We consider a square FG nanoplate with the length a, the width b and the thickness h, which is made from mixture of ceramics and metals as shown in Fig. 1. The material

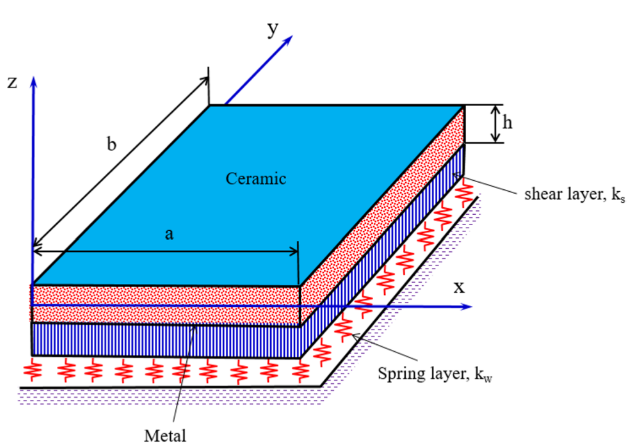

Fig. 1 Model of FG nanoplates resting on two-layer elastic foundations

properties are assumed to change continuously from a top surface ($z = +h/2$) to the bottom ($z = -h/2$) surface according to a power-law distribution. The FG nanoplates rest on elastic foundations via the Pasternak-type consisting of two overlapping layers. The first layer is expressed as a spring system with the stiffness coefficient k_w, and the second layer is the sliding layer represented as parallel lines with a sliding stiffness coefficient k_s.

The effective property of FG material is given by a power law of volume fraction as:

$$\begin{cases} P(z) = P_m + \left(P_c - P_m\right)V_c \\ V_c = \left(\frac{1}{2} + \frac{z}{h}\right)^n \end{cases}, \tag{1}$$

where P is the effective material property such as Young's modulus E, mass density ρ, and Poisson's ratio ν; subscripts m and c denote the metallic and ceramic constituents, respectively; and V_c is the volume-fractions of the ceramic, n is the volume-fraction exponent. The volume-fractions of ceramic and metal varying through the thickness via the volume-fraction exponents n are illustrated in Fig. 2.

2.2 Nonlocal elastic theory

In the classical elasticity theories, the stress tensor at any point only depends on the strain tensor at that point. However, in the nonlocal continuum theory, the stress tensor at a point depends on the strain tensor at all the points of the continuum. According to the nonlocal theory proposed by Eringen [3], the nonlocal constitutive relation of a Hooke solid is given by:

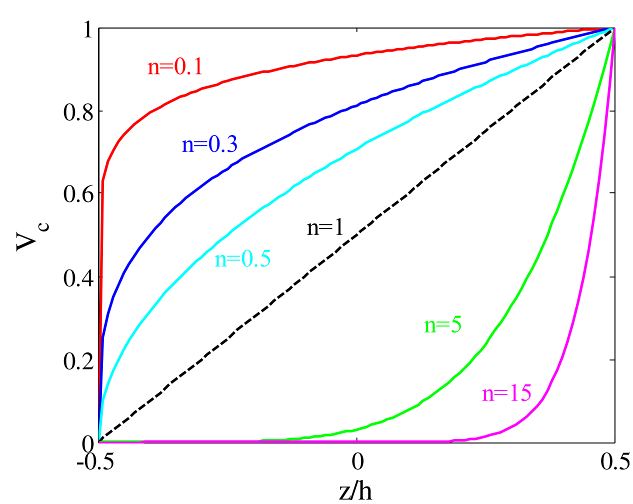

Fig. 2 Variation of the volume fraction versus the dimensionless thickness

$$\sigma_{ij} - \mu\nabla^2\sigma_{ij} = \sigma_{ij}^l$$
$$\sigma_{ij}^l = C_{ijkl}\varepsilon_{ij};\mu = (e_0 l)^2, \tag{2}$$

where σ_{ij} is the nonlocal stress tensor; σ_{ij}^l is the local stress tensor; C_{ijkl} is the elastic constant-coefficient; ε_{ij} is the local strain tensor; μ represents the small-scale effect in nanostructures; l is an internal characteristic length and e_0 is a constant. $\nabla^2 = \frac{\partial^2}{\partial x^2} + \frac{\partial^2}{\partial y^2}$ is the two-dimensional Laplacian operator.

2.3 Four-unknown hyperbolic sine shear deformation theory

In present work, the displacement field at any point of the FG nanoplate (U_1, U_2, U_3) is written as [53]:

$$\begin{cases} U_1(x,y,z,t) = u_0(x,y,t) - z\frac{\partial w^b}{\partial x} - f(z)\frac{\partial w^s}{\partial x} \\ U_2(x,y,z,t) = v_0(x,y,t) - z\frac{\partial w^b}{\partial y} - f(z)\frac{\partial w^s}{\partial y} \\ U_3(x,y,z,t) = w^b + w^s \end{cases} \tag{3}$$

$$f(z) = z - \psi(z); \psi(z) = h \times \sinh\left(\frac{z}{h}\right) - z \times \cosh\left(\frac{1}{2}\right), \tag{4}$$

where U_1, U_2, U_3 are the displacements in the x, y, and z directions, respectively; u_0 and v_0 are respectively the in-plane displacements of the middle surface; w^b and w^s are the bending and shear components of the transverse displacement, respectively. In the general case, the various four unknowns of the displacements u_0, v_0, w^b and w^s are the function depending on the variables x and y.

The linear strain components of the FG nanoplate are written based on the displacements field in Eq. (3) as follows:

$$\varepsilon_{xx} = \frac{\partial U_1}{\partial x} = \frac{\partial u_0}{\partial x} - z\frac{\partial^2 w^b}{\partial x^2} - f(z)\frac{\partial^2 w^s}{\partial x^2} = u_{0,x} - zw^b_{,xx} - f(z)w^s_{,xx} \tag{5}$$

$$\varepsilon_{yy} = \frac{\partial U_2}{\partial y} = \frac{\partial v_0}{\partial y} - z\frac{\partial^2 w^b}{\partial y^2} - f(z)\frac{\partial^2 w^s}{\partial y^2} = v_{0,y} - zw^b_{,yy} - f(z)w^s_{,yy} \tag{6}$$

$$\varepsilon_{xy} = \frac{\partial U_1}{\partial y} + \frac{\partial U_2}{\partial x} = \frac{\partial u_0}{\partial y} + \frac{\partial v_0}{\partial x} - 2z\frac{\partial^2 w^b}{\partial x\partial y} - 2f(z)\frac{\partial^2 w^s}{\partial x\partial y} = u_{0,y} + v_{0,x} - 2zw^b_{,xy} - 2f(z)w^s_{,xy} \tag{7}$$

$$\gamma_{xz} = \frac{\partial U_1}{\partial z} + \frac{\partial U_3}{\partial x} = g(z)\frac{\partial w^s}{\partial x} = g(z)w^s_{,x} \tag{8}$$

$$\gamma_{yz} = \frac{\partial U_2}{\partial z} + \frac{\partial U_3}{\partial y} = g(z)\frac{\partial w^s}{\partial y} = g(z)w^s_{,y}, \tag{9}$$

where

$$g(z) = \frac{\partial\psi(z)}{\partial z} = \cosh\left(\frac{z}{h}\right) - \cosh\left(\frac{1}{2}\right). \tag{10}$$

In Eqs. (8) and (9), the components of the transverse shear strainsγ_{xz},γ_{yz} are equal to zero on top $(z = +h/2)$ and bottom surfaces $(z = -h/2)$ of the FG nanoplate. These formulations can be briefed as vectors as follows:

$$\boldsymbol{\varepsilon} = \begin{Bmatrix} \varepsilon_{xx} \\ \varepsilon_{yy} \\ \varepsilon_{xy} \end{Bmatrix} = \boldsymbol{\varepsilon}^0 + z\boldsymbol{\varepsilon}^1 + f(z)\boldsymbol{\varepsilon}^2; \boldsymbol{\gamma} = \begin{Bmatrix} \gamma_{xz} \\ \gamma_{yz} \end{Bmatrix} = g(z)\boldsymbol{\gamma}^0, \tag{11}$$

where

$$\boldsymbol{\varepsilon}^0 = \begin{Bmatrix} u_{0,x} \\ v_{0,y} \\ u_{0,y} + v_{0,x} \end{Bmatrix}; \boldsymbol{\varepsilon}^1 = -\begin{Bmatrix} w^b_{,xx} \\ w^b_{,yy} \\ 2w^b_{,xy} \end{Bmatrix};$$
$$\boldsymbol{\varepsilon}^2 = -\begin{Bmatrix} w^s_{,xx} \\ w^s_{,yy} \\ 2w^s_{,xy} \end{Bmatrix}; \gamma^0 = \begin{Bmatrix} w^s_{,x} \\ w^s_{,y} \end{Bmatrix}. \tag{12}$$

According to the nonlocal elasticity model in Eq. (2), the constitutive relations (between nonlocal stresses and strains) for elastic nanoplates can be given as follows:

$$\begin{Bmatrix} \sigma_{xx} - \mu\nabla^2\sigma_{xx} \\ \sigma_{yy} - \mu\nabla^2\sigma_{yy} \\ \sigma_{xy} - \mu\nabla^2\sigma_{xy} \\ \sigma_{xz} - \mu\nabla^2\sigma_{xz} \\ \sigma_{yz} - \mu\nabla^2\sigma_{yz} \end{Bmatrix} = \begin{Bmatrix} C_{11} & C_{12} & 0 & 0 & 0 \\ C_{12} & C_{22} & 0 & 0 & 0 \\ 0 & 0 & C_{66} & 0 & 0 \\ 0 & 0 & 0 & C_{55} & 0 \\ 0 & 0 & 0 & 0 & C_{44} \end{Bmatrix} \begin{Bmatrix} \varepsilon_{xx} \\ \varepsilon_{yy} \\ \varepsilon_{xy} \\ \gamma_{xz} \\ \gamma_{yz} \end{Bmatrix} = \begin{bmatrix} \mathbf{D}_b & 0 \\ 0 & \mathbf{D}_s \end{bmatrix} \begin{Bmatrix} \boldsymbol{\varepsilon} \\ \boldsymbol{\gamma} \end{Bmatrix} \tag{13}$$

in which C_{ij} can be expressed as:

$$C_{11} = C_{22} = \frac{E(z)}{1 - v(z)^2}; C_{12} = \frac{v(z)E(z)}{1 - v(z)^2}; C_{66} = C_{55} = C_{44} = \frac{E(z)}{2(1 + v(z))}$$
$$\mathbf{D}_b = \begin{bmatrix} C_{11} & C_{12} & 0 \\ C_{21} & C_{22} & 0 \\ 0 & 0 & C_{66} \end{bmatrix}; \mathbf{D}_s = \begin{bmatrix} C_{55} & 0 \\ 0 & C_{44} \end{bmatrix} \tag{14}$$

Next, the equations of motion of four unknowns using the hyperbolic sine shear deformation theory are derived from Hamilton's principle for the FG nanoplate resting on the elastic foundation as:

$$\int_{t_1}^{t_2} (\delta U + \delta V - \delta W - \delta T)\mathrm{d}t = 0, \tag{15}$$

where δU, δV, δW and δT are the variation of the strain energy of the FG nanoplates, the energy stored in the deformed elastic medium, the work done by applied force and the kinetic energy, respectively. The variation of the strain energy can be given as

$$\delta U=\int_S\int_{-h/2}^{+h/2}\left(\sigma_{xx}\delta\varepsilon_{xx}+\sigma_{yy}\delta\varepsilon_{yy}+\sigma_{xy}\delta\varepsilon_{xy}+\sigma_{xz}\delta\gamma_{xz}+\sigma_{yz}\delta\gamma_{xz}\right)\mathrm{d}z\mathrm{d}S \tag{16}$$

$$=\int_S\left(\begin{array}{l}N_{xx}\frac{\partial\delta u_0}{\partial x}-M_{xx}\frac{\partial^2\delta w^b}{\partial x^2}-L_{xx}\frac{\partial^2\delta w^s}{\partial x^2}+N_{yy}\frac{\partial\delta v_0}{\partial y}-M_{yy}\frac{\partial^2\delta w^s}{\partial y^2}\\-L_{yy}\frac{\partial^2\delta w^s}{\partial y^2}+N_{xy}\left(\frac{\partial\delta u_0}{\partial y}+\frac{\partial\delta v_0}{\partial x}\right)-2M_{xy}\frac{\partial^2\delta w^b}{\partial x\partial y}-\\2L_{xy}\frac{\partial^2\delta w^s}{\partial x\partial y}+Q_{xz}\frac{\partial\delta w^s}{\partial x}+Q_{yz}\frac{\partial\delta w^s}{\partial y}\end{array}\right)\mathrm{d}S. \tag{17}$$

The variation of the energy stored in the deformed elastic foundation is expressed by

$$\delta V=\int_S R\delta\left(w^b+w^s\right)\mathrm{d}S, \tag{18}$$

where $R=k_w\left(w^b+w^s\right)-k_s\nabla^2\left(w^b+w^s\right)$ is the reaction force of an elastic foundation.

The variation of work done by applied force can be expressed by

$$\delta W=\int_S -q(x,y)\delta\left(w^b+w^s\right)\mathrm{d}S \tag{19}$$

The variation of kinetic energy is given by

$$\delta T=\int_S\int_{-h/2}^{+h/2}\rho(z)\left(\dot U_1\delta\dot U_1+\dot U_2\delta\dot U_2+\dot U_3\delta\dot U_3\right)\mathrm{d}z\mathrm{d}S \tag{20}$$

$$=\int_S\left(\begin{array}{l}I_0\left(\dot u_0\delta\dot u_0+\dot v_0\delta\dot v_0+\left(\dot w^b+\dot w^s\right)\delta\left(\dot w^b+\dot w^s\right)\right)-\\I_1\left(\dot u_0\delta\dot w^b_{,x}+\dot w^b_{,x}\delta\dot u_0+\dot v_0\delta\dot w^b_{,y}+\dot w^b_{,x}\delta\dot v_0\right)+I_2\left(\dot w^b_{,x}\delta\dot w^b_{,x}+\dot w^b_{,y}\delta\dot w^b_{,y}\right)-\\J_1\left(\dot u_0\delta\dot w^s_{,x}+\dot w^s_{,x}\delta\dot u_0+\dot v_0\delta\dot w^s_{,y}+\dot w^s_{,y}\delta\dot v_0\right)+K_2\left(\dot w^s_{,x}\delta\dot w^s_{,x}+\dot w^s_{,y}\delta\dot w^s_{,y}\right)+\\J_2\left(\dot w^b_{,x}\delta\dot w^s_{,x}+\dot w^s_{,x}\delta\dot w^b_{,x}+\dot w^b_{,y}\delta\dot w^s_{,y}+\dot w^s_{,y}\delta\dot w^b_{,y}\right)\end{array}\right)\mathrm{d}S, \tag{21}$$

where S is the area of the element.

By substituting Eqs. (16), (18), (19) and (20) into Eq. (15) and integrating by parts, the equations of motion of FG nanoplates can be obtained as:

$$\delta u_0:\ N_{xx,x}+N_{xy,y}=I_0\ddot u_0-I_1\ddot w^b_{,x}-J_1\ddot w^s_{,x} \tag{22}$$

$$\delta v_0:\ N_{yy,y}+N_{xy,x}=I_0\ddot v_0-I_1\ddot w^b_{,y}-J_1\ddot w^s_{,y} \tag{23}$$

$$\begin{aligned}\delta w^b:\ &M_{xx,xx}+2M_{xy,xy}+M_{yy,yy}+q(x,y)-k_w\left(w^b+w^s\right)\\&+k_s\nabla^2\left(w^b+w^s\right)\\&=I_0\left(\ddot w^b+\ddot w^s\right)+I_1\left(\ddot u_{0,x}+\ddot v_{0,y}\right)-I_2\nabla^2\ddot w^b-J_2\nabla^2\ddot w^s\end{aligned} \tag{24}$$

$$\begin{aligned}\delta w^s:\ &L_{xx,xx}+2L_{xy,xy}+L_{yy,yy}+Q_{xz,x}+Q_{yz,y}+q(x,y)-k_w\left(w^b+w^s\right)\\&+k_s\nabla^2\left(w^b+w^s\right)\\&=I_0\left(\ddot w^b+\ddot w^s\right)+J_1\left(\ddot u_{0,x}+\ddot v_{0,y}\right)-J_2\nabla^2\ddot w^b-K_2\nabla^2\ddot w^s,\end{aligned} \tag{25}$$

where the dot (.) superscript convention indicates differentiation with respect to the time variable t; $q(x,y)$ is the transverse load, and (I_i,J_j,K_k) are the mass moment of inertia defined by

$$(I_0,I_1,I_2,J_1,J_2,K_2)=\int_{\frac{-h}{2}}^{\frac{h}{2}}\left(1,z,z^2,f(z),zf(z),f(z)^2\right)\rho(z)\mathrm{d}z. \tag{26}$$

The local stress resultants are given as

$$\left\{N^l_{ij};M^l_{ij};L^l_{ij}\right\}=\int_{\frac{-h}{2}}^{\frac{h}{2}}\sigma^l_{ij}\{1;z;f(z)\}\mathrm{d}z;ij=xx,yy,xy \tag{27}$$

$$\left\{Q^l_{xz};Q^l_{yz}\right\}=\int_{\frac{-h}{2}}^{\frac{h}{2}}\left\{\sigma^l_{xz};\sigma^l_{yz}\right\}g(z)\mathrm{d}z. \tag{28}$$

Substituting Eq. (11) into Eq. (13) and subsequent results into Eqs. (27) and (28), the stress resultants in terms of displacement fields (u_0, v_0, w^b and w^s) for a nonlocal model can be introduced as follows:

$$\left\{N_{xx}N_{yy}N_{xy}\right\}^T-\mu\nabla^2\left\{N_{xx}N_{yy}N_{xy}\right\}^T=\boldsymbol{A}\boldsymbol{\varepsilon}^0+\boldsymbol{B}\boldsymbol{\varepsilon}^1+\boldsymbol{B}^b\boldsymbol{\varepsilon}^2; \tag{29}$$

$$\left\{M_{xx}M_{yy}M_{xy}\right\}^T-\mu\nabla^2\left\{M_{xx}M_{yy}M_{xy}\right\}^T=\boldsymbol{B}\boldsymbol{\varepsilon}^0+\boldsymbol{B}\boldsymbol{\varepsilon}^1+\boldsymbol{F}^b\boldsymbol{\varepsilon}^2; \tag{30}$$

$$\left\{L_{xx}L_{yy}L_{xy}\right\}^T-\mu\nabla^2\left\{L_{xx}L_{yy}L_{xy}\right\}^T=\boldsymbol{B}^b\boldsymbol{\varepsilon}^0+\boldsymbol{F}^b\boldsymbol{\varepsilon}^1+\boldsymbol{H}\boldsymbol{\varepsilon}^2; \tag{31}$$

$$\left\{Q_{xz}Q_{yz}\right\}^{T}-\mu\nabla^{2}\left\{Q_{xz}Q_{yz}\right\}^{T}=\boldsymbol{A}^{b}\boldsymbol{\gamma}^{0};\tag{32}$$

where:

$$\left(\boldsymbol{A},\boldsymbol{B},\boldsymbol{B}^{b},\boldsymbol{F},\boldsymbol{F}^{b},\boldsymbol{H}\right)=\int_{\frac{-h}{2}}^{\frac{h}{2}}\boldsymbol{D}_{b}(1,z,f(z),z^{2},zf(z),f(z)^{2})\mathrm{d}z;\boldsymbol{A}^{b}=\int_{\frac{-h}{2}}^{\frac{h}{2}}\boldsymbol{D}_{s}g^{2}(z)\mathrm{d}z,\tag{33}$$

Next, substituting Eqs. (29)–(33) into Eqs. (22)–(25), the equations of motion can be rewritten in terms of displacements as follows:

$$N_{xx,x}+N_{xy,y}=\left(1-\mu\nabla^{2}\right)\left(I_{0}\ddot{u}_{0}-I_{1}\ddot{w}^{\mathrm{b}}_{,x}-J_{1}\ddot{w}^{\mathrm{s}}_{,x}\right)\tag{34}$$

$$N_{xy,x}+N_{yy,y}=\left(1-\mu\nabla^{2}\right)\left(I_{0}\ddot{v}_{0}-I_{1}\ddot{w}^{\mathrm{b}}_{,y}-J_{1}\ddot{w}^{\mathrm{s}}_{,y}\right)\tag{35}$$

$$\left(1-\mu\nabla^{2}\right)\begin{pmatrix}\left(M_{xx,xx}+2M_{xy,xy}+M_{yy,yy}\right)=\\-q(x,y)+k_{w}\left(w^{\mathrm{b}}+w^{\mathrm{s}}\right)-k_{s}\nabla^{2}\left(w^{\mathrm{b}}+w^{\mathrm{s}}\right)+\\I_{0}\left(\ddot{w}^{\mathrm{b}}+\ddot{w}^{\mathrm{s}}\right)+I_{1}\left(\ddot{u}_{0,x}+\ddot{v}_{0,y}\right)-I_{2}\nabla^{2}\ddot{w}^{\mathrm{b}}-J_{2}\nabla^{2}\ddot{w}^{\mathrm{s}}\end{pmatrix}\tag{36}$$

$$\left(1-\mu\nabla^{2}\right)\begin{pmatrix}L_{xx,xx}+2L_{xy,xy}+L_{yy,yy}+Q_{xz,x}+Q_{yz,y}=\\-q(x,y)+k_{w}\left(w^{\mathrm{b}}+w^{\mathrm{s}}\right)-k_{s}\nabla^{2}\left(w^{\mathrm{b}}+w^{\mathrm{s}}\right)\\+I_{0}\left(\ddot{w}^{\mathrm{b}}+\ddot{w}^{\mathrm{s}}\right)+J_{1}\left(\ddot{u}_{0,x}+\ddot{v}_{0,y}\right)-J_{2}\nabla^{2}\ddot{w}^{\mathrm{b}}-K_{2}\nabla^{2}\ddot{w}^{\mathrm{s}}\end{pmatrix}\tag{37}$$

Finally, the variation form or weak forms can be obtained for Eqs. (34)–(37) by multiplying them with ($\delta u_0, \delta v_0, \delta w^b and \delta w^s$) respectively, and integrating over the element domain S and adding together the same sides of each equation, we obtain the following results

$$\int_{\mathrm{S}}\left(N_{xx}\delta u_{0,x}+N_{xy}\delta u_{0,y}-\left(1-\mu\nabla^{2}\right)\left(I_{0}\ddot{u}_{0}-I_{1}\ddot{w}^{\mathrm{b}}_{,x}-J_{1}\ddot{w}^{\mathrm{s}}_{,x}\right)\delta u_{0}\right)\mathrm{d}S=0\tag{38}$$

$$\int_{\mathrm{S}}\left(N_{xy}\delta v_{0,x}+N_{yy}\delta v_{0,y}-\left(1-\mu\nabla^{2}\right)\left(I_{0}\ddot{v}_{0}-I_{1}\ddot{w}^{\mathrm{b}}_{,y}-J_{1}\ddot{w}^{\mathrm{s}}_{,y}\right)\delta v_{0}\right)\mathrm{d}S=0\tag{39}$$

$$\int_{\mathrm{S}}\begin{pmatrix}M_{xx}\delta w^{\mathrm{b}}_{,xx}+2M_{xy}\delta w^{\mathrm{b}}_{,xy}+M_{yy}\delta w^{\mathrm{b}}_{,yy}-\\\left(1-\mu\nabla^{2}\right)\begin{pmatrix}-q(x,y)+k_{w}\left(w^{\mathrm{b}}+w^{\mathrm{s}}\right)-k_{s}\nabla^{2}\left(w^{E}+w^{\mathrm{E}}\right)+\\I_{0}\left(\ddot{w}^{\mathrm{b}}+\ddot{w}^{\mathrm{s}}\right)+I_{1}\left(\ddot{u}_{0,x}+\ddot{v}_{0,y}\right)-I_{2}\nabla^{2}\ddot{w}^{\mathrm{b}}-J_{2}\nabla^{2}\ddot{w}^{\mathrm{s}}\end{pmatrix}\delta w^{\mathrm{b}}\end{pmatrix}\mathrm{d}S=0\tag{40}$$

$$\int_{\mathrm{S}}\begin{pmatrix}L_{xx}\delta w^{\mathrm{s}}_{,xx}+2L_{xy}\delta w^{\mathrm{s}}_{,xy}+L_{yy}\delta w^{\mathrm{s}}_{,yy}+Q_{xz}\delta w^{\mathrm{s}}_{,x}+Q_{yz}\delta w^{\mathrm{s}}_{,y}-\\\left(1-\mu\nabla^{2}\right)\begin{pmatrix}-q(x,y)+k_{w}\left(w^{b}+w^{\mathrm{s}}\right)-k_{s}\nabla^{2}\left(w^{\mathrm{b}}+w^{s}\right)\\+I_{0}\left(\ddot{w}^{\mathrm{b}}+\ddot{w}^{\mathrm{s}}\right)+J_{1}\left(\ddot{u}_{0,x}+\ddot{v}_{0,y}\right)-J_{2}\nabla^{2}\ddot{w}^{\mathrm{b}}-K_{2}\nabla^{2}\ddot{w}^{\mathrm{s}}\end{pmatrix}\delta w^{s}\end{pmatrix}\mathrm{d}S=0\tag{41}$$

2.4 Finite element formulation

In this work, the four-node plate element with 8 degrees of freedom for each node as shown in Fig. 3 is used, the nodal displacement vector can be defined as follows

$$\boldsymbol{q}_{\mathrm{e}}=\left[\boldsymbol{q}_{1}^{\mathrm{T}}\ \boldsymbol{q}_{2}^{\mathrm{T}}\ \boldsymbol{q}_{3}^{\mathrm{T}}\ \boldsymbol{q}_{4}^{\mathrm{T}}\right]^{\mathrm{T}}\tag{42}$$

The displacements at the node $i,(i=1/4)$ are expressed as:

$$\boldsymbol{q}_{i}=\left\{\ u_{0i}\ v_{0i}\ w^{\mathrm{b}}_{i}\ w^{\mathrm{s}}_{i}\ w^{\mathrm{b}}_{i,x}\ w^{\mathrm{s}}_{i,x}\ w^{\mathrm{b}}_{i,y}\ w^{\mathrm{s}}_{i,y}\ \right\}\tag{43}$$

The displacement field of the plate element is interpolated through the displacement node as:

$$\begin{cases}u_{0}=\boldsymbol{N}_{u}\boldsymbol{q}_{e};v_{0}=\boldsymbol{N}_{v}\boldsymbol{q}_{e};w^{\mathrm{b}}=\boldsymbol{N}_{wb}\boldsymbol{q}_{e};w^{\mathrm{s}}=\boldsymbol{N}_{ws}\boldsymbol{q}_{e};\\w^{\mathrm{b}}_{i,x}=\boldsymbol{N}_{wb,x}\boldsymbol{q}_{e};w^{\mathrm{b}}_{i,y}=\boldsymbol{N}_{wb,y}\boldsymbol{q}_{e};w^{\mathrm{s}}_{i,x}=\boldsymbol{N}_{ws,x}\boldsymbol{q}_{e};w^{\mathrm{s}}_{i,y}=\boldsymbol{N}_{ws,y}\boldsymbol{q}_{e}\end{cases},\tag{44}$$

where $\boldsymbol{N}_u, \boldsymbol{N}_v, \boldsymbol{N}_{wb}, \boldsymbol{N}_{ws}$ are the shape functions with size (1×32)

$$\begin{cases}N_{u}=\left[N_{1}^{(1)}\ N_{2}^{(1)}\ N_{3}^{(1)}\ N_{4}^{(1)}\right];\ N_{v}=\left[N_{1}^{(2)}\ N_{2}^{(2)}\ N_{3}^{(2)}\ N_{4}^{(2)}\right];\\N_{wb}=\left[N_{1}^{(3)}\ N_{2}^{(3)}\ N_{3}^{(3)}\ N_{4}^{(3)}\right];\ N_{ws}=\left[N_{1}^{(4)}\ N_{2}^{(4)}\ N_{3}^{(4)}\ N_{4}^{(4)}\right];\end{cases}\tag{45}$$

The shape functions $N_i^{(j)}(j = 1 \div 4)$ in Eq. (45) have the size (1×8)

$$\begin{cases} N_i^{(1)} = \{ \lambda_i \ 0\ 0\ 0\ 0\ 0\ 0\ 0 \}; \\ N_i^{(2)} = \{ 0\ \lambda_i\ 0\ 0\ 0\ 0\ 0\ 0 \}; \\ N_i^{(3)} = \{ 0\ 0\ \hbar_{3i-2}\ 0\ \hbar_{3i-1}\ 0\ \hbar_{3i}\ 0 \}; \\ N_i^{(4)} = \{ 0\ 0\ 0\ \hbar_{3i-2}\ 0\ \hbar_{3i-1}\ 0\ \hbar_{3i} \}. \end{cases}, \tag{46}$$

where $\lambda_i(i = 1 \div 4)$ is the Lagrange interpolation functions and $\hbar_k(k = 1 \div 12)$ is the Hermit interpolation functions. The functions are given by Appendix A.

Next, substituting Eq. (44) into Eqs. (38) and (41), the finite element model for the static and vibration analysis of the FG nanoplates resting on the elastic foundation, respectively, can be expressed as:

$$\boldsymbol{M}_e \ddot{\boldsymbol{q}}_e + \boldsymbol{K}_e \boldsymbol{q}_e = 0, \tag{47}$$

$$\boldsymbol{K}_e \boldsymbol{q}_e = \boldsymbol{P}_e \tag{48}$$

in which $\boldsymbol{K}_e$ represent the stiffness matrices; $\boldsymbol{M}_e$ is the mass matrices and $\boldsymbol{P}_e$ is the load vector of each nanoplate element and the matrices are computed as:

$$\boldsymbol{K}_e = \boldsymbol{K}_e^{\mathrm{b}} + \boldsymbol{K}_e^{\mathrm{s}} + \boldsymbol{K}_e^{\mathrm{fou}} \tag{49}$$

with

$$\boldsymbol{K}_e^{\mathrm{b}} = \int\limits_S \left[\boldsymbol{B}_1^{\mathrm{T}}\ \boldsymbol{B}_2^{\mathrm{T}}\ \boldsymbol{B}_3^{\mathrm{T}} \right] \begin{bmatrix} \boldsymbol{A} & \boldsymbol{B} & \boldsymbol{B}^{\mathrm{b}} \\ \boldsymbol{B} & \boldsymbol{F} & \boldsymbol{F}^{\mathrm{b}} \\ \boldsymbol{B}^{\mathrm{b}} & \boldsymbol{F}^{\mathrm{b}} & \boldsymbol{H} \end{bmatrix} \begin{bmatrix} \boldsymbol{B}_1 \\ \boldsymbol{B}_2 \\ \boldsymbol{B}_3 \end{bmatrix} \mathrm{d}S \tag{50}$$

$$\boldsymbol{K}_e^{\mathrm{s}} = \int\limits_S \left(\boldsymbol{B}_1^{\mathrm{b}}\right)^{\mathrm{T}} \boldsymbol{A}^{\mathrm{b}} \boldsymbol{B}_1^{\mathrm{b}} \mathrm{d}S \tag{51}$$

$$\boldsymbol{K}_e^{\mathrm{fou}} = \int\limits_S \begin{pmatrix} k_w \left[\boldsymbol{B}_w^{\mathrm{T}} \boldsymbol{B}_w + \mu \left(\boldsymbol{B}_{wx}^{\mathrm{T}} \boldsymbol{B}_{wx} + \boldsymbol{B}_{wy}^{\mathrm{T}} \boldsymbol{B}_{wy} \right) \right] + k_s \left(\boldsymbol{B}_{wx}^{\mathrm{T}} \boldsymbol{B}_{wx} + \boldsymbol{B}_{wy}^{\mathrm{T}} \boldsymbol{B}_{wy} \right) \\ + \mu k_s \left(\boldsymbol{B}_{wx2}^{\mathrm{T}} \boldsymbol{B}_{wx2} + \boldsymbol{B}_{wy2}^{\mathrm{T}} \boldsymbol{B}_{wy2} + \boldsymbol{B}_{wx2}^{\mathrm{T}} \boldsymbol{B}_{wy2} + \boldsymbol{B}_{wy2}^{\mathrm{T}} \boldsymbol{B}_{wx2} \right) \end{pmatrix} \mathrm{d}S \tag{52}$$

$$\boldsymbol{M}_e = \int\limits_S \left[\boldsymbol{N}^{\mathrm{T}} \boldsymbol{D}_m \boldsymbol{N} + \mu \left(\boldsymbol{N}_x^{\mathrm{T}} \boldsymbol{D}_m \boldsymbol{N}_x + \boldsymbol{N}_y^{\mathrm{T}} \boldsymbol{D}_m \boldsymbol{N}_y \right) \right] \mathrm{d}S \tag{53}$$

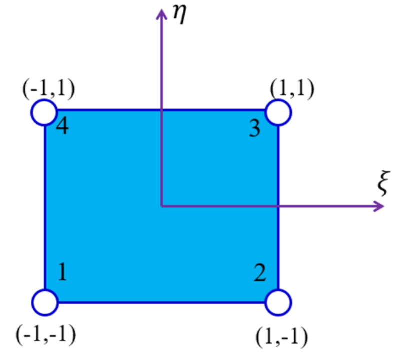

Fig. 3 Four-node element plate

$$\begin{aligned} \boldsymbol{P}_e &= \int\limits_S \left(1 - \mu \nabla^2\right) q(x, y) \boldsymbol{B}_w^T \mathrm{d}S \\ &= \int\limits_S q \boldsymbol{B}_w^T \mathrm{d}S - \mu \int\limits_S q(x, y) \left(\boldsymbol{B}_{w,xx}^T + \boldsymbol{B}_{w,yy}^T \right) \mathrm{d}S \\ &\quad - \mu \int\limits_S \boldsymbol{B}_w^T \left(q_{,xx}(x, y) + q_{,yy}(x, y) \right) \mathrm{d}S \end{aligned} \tag{54}$$

in which the unknown variables are the strain matrices and defined in Appendix B.

3 Numerical results and discussions

In this section, several numerical examples are performed to investigate the influences of some geometric parameters, material properties, the elastic foundations, the nonlocal parameters and the various boundary conditions on the responses of the bending and the free vibration of FG nanoplates resting on the elastic foundation. In most examples of this paper, the FG nanoplates are made from the material properties: Al/Al_2O_3 with the ceramics are Al_2O_3; Al represents the metals. The length of the nanoplates is $a = 10$ nm. For finite element analysis, this work uses Gauss integral

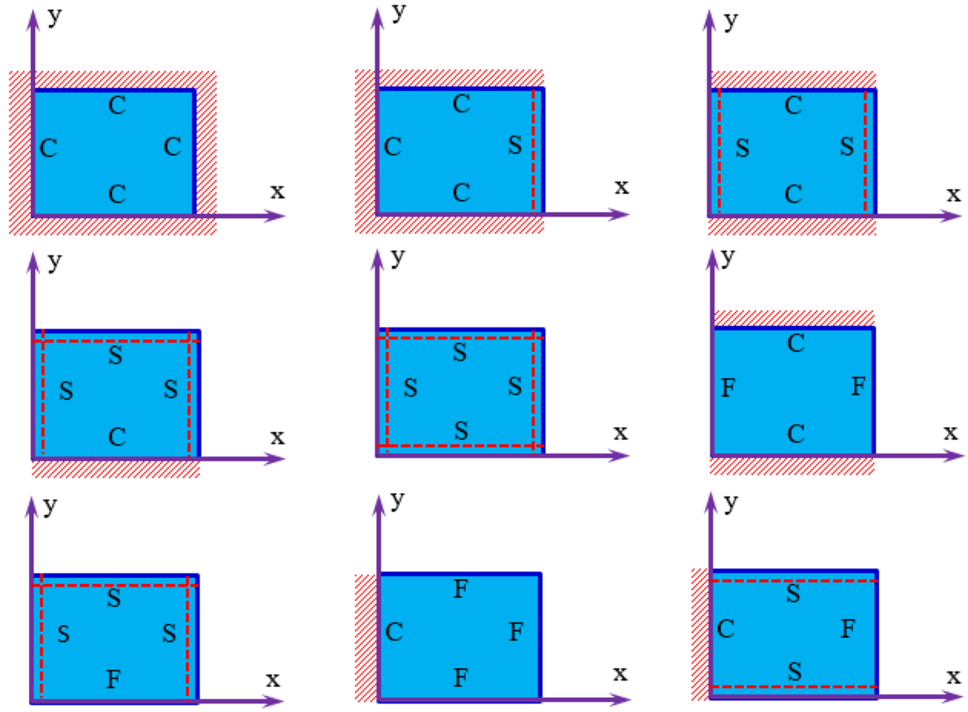

Fig. 4 Boundary conditions of the nanoplates

2×2 to calculate the stiffness matrices, the mass matrices and the load vector of the nanoplate elements. The boundary condition symbols are used in this study: C (clamped), S (simple supported), and F (free) as shown in Fig. 4.

For convenience in comparing its numerical results with the exact solutions in the literature, the following dimensionless forms are given:

$$w^{**} = w_{\max} \times \frac{100E_c h^3}{q_0 a^4}; w_1 = w_{\max} \times \frac{100E_c h^3}{12(1-\nu^2)q_0 a^4}; \sigma_{xx}^{**}(z) = \frac{10h}{q_0 a}\sigma_{xx}\left(\frac{a}{2},\frac{b}{2},z\right);$$

$$\sigma_{xy}^{**}(z) = \frac{10h}{q_0 a}\sigma_{xy}(0,0,z); \sigma_{xz}^{**}(z) = \frac{10h}{q_0 a}\sigma_{xz}\left(0,\frac{b}{2},z\right);$$

$$\Omega^* = \omega_{11}\frac{a^2}{h}\sqrt{\rho_c/E_c}; \Omega = \omega_{11}h\sqrt{\rho_m/E_m}; \Omega_1 = \omega_{11}h\sqrt{\rho_c/E_c}$$

$$K_w = \frac{(k_w a^4)}{D_c}; K_s = \frac{(k_s a^2)}{D_c}; K_w1 = \frac{(k_w a^4)}{D_m}; K_s1 = \frac{(k_s a^2)}{D_m}; D_c = \frac{(E_c h^3)}{12(1-\nu_c^2)}; D_m = \frac{(E_m h^3)}{12(1-\nu_m^2)}$$

The sinusoidal distributed load has the form of $q(x,y) = q_0 sin(\frac{\pi x}{a})sin(\frac{\pi y}{b}), where q_0$ is the maximum load at the central point of the plate.

3.1 Convergence and accuracy study

Before evaluating the accuracy and the convergence of the present finite formulation for analysis of FG nanoplates, this part conducts some analysis of the FG plates and compares their results with those available in the literature. Firstly, we investigate the bending and free vibration responses of the simply supported FG plate (the length $a = 10$ and $h = 1$) subjected to the sinusoidal load. Table 1 provides the results of dimensionless deflection w_1 by the proposed method for the uniform meshes $2\times2, 4\times4.8\times8.10\times10.16\times16$ and 20×20 and compared with the results by Thai et al. [55, 56]. From Table 1, it is observed that the numerical results of the bending and free vibration responses of the present method agree well with those given in Ref [55]. with mesh size 10×10, and those in Ref [56]. with mesh size 8×8, respectively. Hence in this paper, the model of the nanoplates will use the mesh size 10×10 and 8×8 for the bending and the free vibration analysis, respectively.

Table 1 The convergence of dimensionless deflection w_1 and fundamental frequency Ω_1 of SSSS square plate under sinusoidal loads ($a/h = 10$)

Mesh	Power-law index (n)			
	Dimensionless deflection w_1			
	0	1	4	10
2×2	0.3918	0.7511	1.1143	1.3077
4×4	0.3111	0.6145	0.9187	1.0558
8×8	0.2976	0.5910	0.8844	1.0129
10×10	0.2964	0.5889	0.8813	1.0090
16×16	0.2953	0.5870	0.8785	1.0054
20×20	0.2951	0.5867	0.8779	1.0047
Navier's [55]	0.2961	0.5890	0.8815	1.0087
Fundamental frequency Ω_1				
2×2	0.0544	0.0420	0.0363	0.0345
4×4	0.0568	0.0436	0.0376	0.0359
8×8	0.0576	0.0442	0.0381	0.0364
10×10	0.0577	0.0442	0.0381	0.0364
16×16	0.0578	0.0443	0.0382	0.0365
20×20	0.0578	0.0443	0.0382	0.0365
Navier's [56]	0.0577	0.0442	0.0381	0.0364

Next, Table 2 presents the numerical results of the dimensionless central deflections w^{**}, the dimensionless in-plane normal stress $\sigma_{xx}^{**}(h/2)$, the dimensionless in-plane shear stress $\sigma_{xy}^{**}(-h/3)$ and the dimensionless transverse shear stress $\sigma_{xz}^{**}(0)$ of the simply supported Al_2O_3/Al square plate (with the length and thickness ratio $a/h = 10$) subjected to sinusoidal load with the volume-fraction exponent varying from 0 to 5 ($n = 0, 1, 2, 5$) and the various foundation stiffness K_w and K_s. It is found that the present results match well with the exact solution produced by Ameur et al. [57].

Next, Table 3 shows the numerical results of the dimensionless center deflection of the isotropic nanoplates subjected to the uniform load $q_0 = 1$. The nanoplate has the length and thickness ratio $a/h = 10$, width-to-length ratio $b/a = 1, 2$; and the material properties $E = 30 \times 10^6, \nu = 0.3$. The results of the proposed method are compared with the Navier's exact solution of Aghababaei and Reddy [58]. It is seen that the present results are in a good agreement with those given in Ref.[58].

Next, Table 4 displays the numerical results of the dimensionless frequency Ω of the square FG nanoplates made from $Si_3N_4/SU_3S_3O_4$ as given in Table 5. The FG nanoplates have the length-to-thickness ratio ($a/h = 5, 10, 20, 50$), the nonlocal coefficient $\mu = 0/4$ and the volume-fraction exponent varies from 0 and ∞ ($n = 0, 1, 5, \infty$). It can be seen that the present results agree well with the Navier's exact solutions performed by Sobhy [59]. Table 6 shows the results of the dimensionless frequency Ω of the square FG nanoplates with aluminum at the bottom surface and zirconia at the top surface (Al/Al_2O_3) resting on the elastic foundation. The various foundation stiffness coefficient K_{w1}, K_{s1}, the volume-fraction exponent n ($n = 0.5 and 2$), the nonlocal coefficient $\mu = 1$ and length-to-thickness ratio $a/h = 5$ are examined in this table. It can be found that the increase of the elastic foundation stiffness leads to the increase of the dimensionless fundamental frequency Ω and the increase of the volume-fraction exponents n leads to the reduce of the dimensionless fundamental frequency Ω. This implies that the increase of the volume-fraction exponents n makes the FG nanoplates become weaker. It is seen again that the present finite element formulation shows a very good agreement with those produced by Panyatong et al. [60].

Through the above-compared results, it can be found that the proposed finite element formulation is accurate and reliable. In addition, it is suitable for analysis of the thick and thin nanoplates which do not requirement any shear correction factor.

3.2 Static bending problem

This sub-section investigates the effects of the nonlocal coefficient μ, the elastic foundation stiffnesses K_w, K_s, the volume-fraction exponent n and the geometric parameters such as length-to-thickness ratio (a/h), width-to-length ratio b/a), the various boundary conditions on the maximum deflection w^{**}, the in-plane normal stress $\sigma_{xx}^{**}(z)$, the in-plane shear stress $\sigma_{xy}^{**}(z)$ and the transverse shear stress $\sigma_{xz}^{**}(z)$ of the FG nanoplates resting on elastic foundation. The material properties of FG nanoplates are given in Table 5.

Table 3 presents the results of the dimensionless central deflection w^{**} and comparison with those given by Aghababaei and Reddy [58]. In addition, Table 3 also shows the values of the in-plane normal stress $\sigma_{xx}^{**}(h/2)$, the in-plane shear stress $\sigma_{xy}^{**}(-h/3)$ and the transverse shear stress $\sigma_{xz}^{**}(0)$. It is seen that the obtained results agree well with published results in Ref.[58]. It is also found that the increase of the nonlocal coefficient μ leads to the increase of the transverse displacements, the in-plane normal stress, the in-plane shear stress and the transverse shear stress. This is because the increase of the nonlocal coefficient μ leads to the larger detachment of the distance between molecules and thus makes the structural stiffness decrease.

Table 2 The dimensionless deflection of the simply supported FG plate resting on the elastic foundation under the sinusoidal distributed load

n	K_w	K_s	Method	$\frac{w^{**}}{10}$	$\frac{\sigma_{xx}^{**}(h/2)}{10}$	$\frac{\sigma_{xy}^{**}(-h/3)}{10}$	$\frac{\sigma_{xz}^{**}(0)}{10}$
0	0	0	[57]	0.2960	1.9955	0.7065	0.2461
			This work	0.2962	1.9866	0.7131	0.2440
	100	0	[57]	0.2328	1.5699	0.5558	0.1936
			This work	0.2330	1.5627	0.5610	0.1883
	0	10	[57]	0.1928	1.2999	0.4602	0.1603
			This work	0.1929	1.2939	0.4644	0.1594
	100	10	[57]	0.1638	1.1048	0.3912	0.1362
			This work	0.1639	1.0996	0.3947	0.1385
1	0	0	[57]	0.5889	3.0869	0.6110	0.2461
			This work	0.5892	3.0703	0.6159	0.2476
	100	0	[57]	0.3825	2.0054	0.3970	0.1337
			This work	0.3827	1.9943	0.4001	0.1414
	0	10	[57]	0.2852	1.4952	0.2959	0.1192
			This work	0.2853	1.4869	0.2983	0.1154
	100	10	[57]	0.2261	1.1855	0.2347	0.0945
			This work	0.2262	1.1789	0.2365	0.0936
2	0	0	[57]	0.7573	3.6093	0.5441	0.2265
			This work	0.7555	3.5849	0.5489	0.2250
	100	0	[57]	0.4472	2.1312	0.3213	0.1337
			This work	0.4465	2.1190	0.3244	0.1393
	0	10	[57]	0.3197	1.5236	0.2297	0.0956
			This work	0.3194	1.5155	0.2320	0.0982
	100	10	[57]	0.2473	1.1785	0.1777	0.0740
			This work	0.2471	1.1726	0.1795	0.0725
5	0	0	[57]	0.9118	4.2488	0.5754	0.2016
			This work	0.9118	4.2071	0.5814	0.1998
	100	0	[57]	0.4969	2.3154	0.3136	0.1099
			This work	0.4939	2.3043	0.3185	0.1066
	0	10	[57]	0.3443	1.6043	0.2173	0.0762
			This work	0.3429	1.5996	0.2211	0.0732
	100	10	[57]	0.2618	1.2197	0.1652	0.0579
			This work	0.2609	1.2174	0.1682	0.0565

Table 7 and Table 8 show the dimensionless central deflection w^{**} and the in-plane normal stress $\sigma_{xx}^{**}(h/2)$ of the simply supported nanoplates resting on the elastic foundation subjected to the uniform distribution load and the sinusoidal distribution load, respectively. The variation of the elastic foundation coefficient, the volume-fraction exponent ($n = 0.5, 1, 5, 10$) and the nonlocal coefficient μ (from 0 to 4) are examined in these tables. The results show that the values of the dimensionless central deflection w^{**} and the in-plane normal stress $\sigma_{xx}^{**}(h/2)$ of the FG nanoplates without resting on elastic foundation increase rapidly as the nonlocal coefficient μ and the volume-fraction exponent n increase. However, it is noted for the case of the FG nanoplates resting on the elastic foundation that the dimensionless central deflection w^{**} and the in-plane normal stress $\sigma_{xx}^{**}(h/2)$ increase slowly versus to the increase of the elastic foundation coefficient. It is observed that the elastic foundation makes the nanoplates become much harder and hence makes both the displacement and stress of nanoplates decrease.

Let us next consider the FG nanoplates with the length-to-thickness ratio $a/h = 10$ resting on the elastic foundation with the foundation stiffness $K_w = K_s = 10$ under the sinusoidally distributed load. Table 9 shows the influence of the boundary conditions on the dimensionless central deflection w^{**} of the

Table 3 The dimensionless deflection and stress of the simply supported isotropic nanoplates versus to the variation of length-to-width ratio and nonlocal coefficient under the sinusoidal distributed load

Method		w^{**}		$\sigma_{xx}^{**}(h/2)$	$\sigma_{xy}^{**}(-h/3)$	$\sigma_{xz}^{**}(0)$
		[58]	This work	This work	This work	This work
b/a	μ	$a/h=10$				
1	0	4.1853	4.2667	2.8840	1.3122	0.4708
	0.5	4.5607	4.6157	3.0775	1.6177	0.7560
	1.0	4.9362	4.9647	3.2711	1.9232	1.0411
	1.5	5.3116	5.3137	3.4647	2.2287	1.3263
	2.0	5.6871	5.6627	3.6583	2.5342	1.6114
	2.5	6.0625	6.0116	3.8519	2.8397	1.8965
	3.0	6.4380	6.3606	4.0454	3.1452	2.1817
2	0	0.7169	0.7152	0.6950	0.4680	0.2405
	0.5	0.8767	0.8683	0.8069	0.7517	0.5219
	1.0	1.0364	1.0272	0.9187	1.0355	0.8032
	1.5	1.1961	1.1861	1.0306	1.3192	1.0845
	2.0	1.3558	1.3450	1.1424	1.6030	1.3659
	2.5	1.5155	1.5039	1.2543	1.8867	1.6472
	3.0	1.6752	1.6728	1.3661	2.1704	1.9285

Table 4 The dimensionless fundamental frequency Ω of the simply supported FG nanoplates versus to the variation of the volume-fraction exponent n, the nonlocal coefficient μ and the length- to-thickness ratio a/h

a/h	μ	Si_3N_4		$n=1$		$n=5$		$SU_3S_3O_4$	
		[59]	This work	[59]	This work	[59]	This work	[59]	This work
5	0	5.10702	5.11002	3.01860	3.02108	2.42443	2.43619	2.11261	2.11650
	0.25	4.98549	4.98841	2.94677	2.94919	2.36674	2.37821	2.06234	2.06613
	1	4.66713	4.66986	2.75859	2.76086	2.21560	2.22634	1.93064	1.93419
	2.25	4.24976	4.25224	2.51190	2.51396	2.01747	2.02724	1.75799	1.76122
	4	3.81763	3.81986	2.25648	2.25833	1.81232	1.82110	1.57923	1.58213
10	0	1.38829	1.38957	0.82250	0.82372	0.66485	0.66676	0.57695	0.57825
	0.25	1.35525	1.35650	0.80292	0.80412	0.64903	0.65089	0.56322	0.56449
	1	1.26871	1.26987	0.75165	0.75277	0.60758	0.60932	0.52725	0.52845
	2.25	1.15525	1.15631	0.68443	0.68545	0.55325	0.55483	0.48010	0.48119
	4	1.03778	1.03873	0.61484	0.61575	0.49699	0.49842	0.43128	0.43226
20	0	0.35558	0.35594	0.21083	0.21118	0.17077	0.17114	0.14799	0.14835
	0.25	0.34712	0.34747	0.20581	0.20616	0.16671	0.16707	0.14447	0.14482
	1	0.32495	0.32528	0.19267	0.19299	0.15606	0.15640	0.13524	0.13557
	2.25	0.32495	0.29619	0.17544	0.17573	0.14210	0.14241	0.12315	0.12344
	4	0.26581	0.26607	0.15760	0.15786	0.12765	0.12793	0.11063	0.11089
50	0	0.05730	0.05736	0.03398	0.03404	0.02754	0.02759	0.02385	0.02392
	0.25	0.05593	0.05599	0.03317	0.03323	0.02688	0.02694	0.02329	0.02335
	1	0.05236	0.05242	0.03105	0.03111	0.02517	0.02522	0.02180	0.02186
	2.25	0.04768	0.04773	0.02827	0.02833	0.02291	0.02296	0.01985	0.01990
	4	0.04283	0.04287	0.02540	0.02545	0.02058	0.02063	0.01783	0.01788

Table 5 Material properties of the FG nanoplates

Properties 1	E(GPa)	v	ρ(kg/m^3)	Properties 2	E(GPa)	v	ρ(kg/m^3)
Si_3N_4	348.43	0.24	2370	Al_2O_3	390	0.30	3800
$SU_3S_3O_4$	201.04	0.30	8166	Al	70	0.30	2707

Table 6 The dimensionless fundamental frequency Ω of the simply supported FG nanoplates versus to the variation of the volume-fraction exponent n and the elastic foundation coefficient ($\mu = 1, a/h = 5, SSSS$)

K_{w1}	K_{s1}	$n=0$	$n=0.5$		$n=2$		$n=5$	$n=\infty$
		This work	[60]	This work	[60]	This work	This work	This work
0	0	0.3788	0.3282	0.3241	0.2671	0.2664	0.2475	0.1930
	10	0.4040	0.3597	0.3556	0.3089	0.3068	0.2939	0.2531
	50	0.4889	0.4650	0.4578	0.4378	0.4307	0.4278	0.3731
10	0	0.3801	0.3299	0.3258	0.2694	0.2687	0.2501	0.1966
	10	0.4052	0.3613	0.3572	0.3109	0.3088	0.2961	0.2559
	50	0.4899	0.4662	0.4590	0.4392	0.4321	0.4293	0.3731
50	0	0.3854	0.3365	0.3325	0.2783	0.2777	0.2603	0.2104
	10	0.4101	0.3673	0.3633	0.3186	0.3166	0.3047	0.2666
	50	0.4940	0.4709	0.4638	0.4447	0.4377	0.4352	0.3731
100	0	0.3918	0.3445	0.3407	0.2890	0.2885	0.2725	0.2264
	10	0.4162	0.3747	0.3708	0.3281	0.3261	0.3152	0.2794
	50	0.4990	0.4766	0.4696	0.4515	0.4446	0.4426	0.3731

FG nanoplates. The obtained results of FG nanoplates with the different boundary conditions can help fill in the gap that the analytical method is missing in published works. The values of displacement decrease gradually corresponding to the following order of boundary conditions: CFFF, CCFF, SSSS, CFCF, CSSS, CCCS, CCCC.

Table 10 presents the values of the dimensionless central deflection w^{**} of the FG nanoplates resting on the elastic foundation with the foundation stiffness $K_w = 30; K_s = 10$ subjected to sinusoidally distributed load. We consider the FG nanoplates with the volume-fraction exponent $n = 1$, the change of nonlocal coefficient, the length-to-thickness ratio and the various boundary conditions. it can be observed that the increase of the nonlocal coefficient and the volume-fraction exponent n leads to the increase of the dimensionless central deflection. In addition, it can be seen that the present finite element method eliminates the shear locking phenomenon and obtains good results when the thickness of the FG nanoplates becomes very thin.

Figure 5 illustrates the dimensionless central deflection w^{**}, the in-plane normal stress $\sigma_{xx}^{**}(z)$, the in-plane shear stress $\sigma_{xy}^{**}(z)$ and the transverse shear stress $\sigma_{xz}^{**}(z)$ of the simply supported FG nanoplates resting on the elastic foundation. In Fig. 5a, it can be seen that the dimensionless central deflections of the FG nanoplates increase rapidly corresponding to the increase of the volume-fraction exponent n from 0 to 2. However, they increase more slowly corresponding to the increase of the volume-fraction exponent n from 2 to 10. Figure 5b, Fig. 5c and Fig. 5d depict the in-plane normal stress $\sigma_{xx}^{**}(z)$, the in-plane shear stress $\sigma_{xy}^{**}(z)$ and the transverse shear stress $\sigma_{xz}^{**}(z)$ at points on the vertical line passing through the centroid of FG nanoplates with $a/h = 10$. It is noted that the values of the in-plane normal stress $\sigma_{xx}^{**}(z)$, the in-plane shear stress $\sigma_{xy}^{**}(z)$ are not equal zero at the point $z/h = 0$ in Fig. 5b and Fig. 5c. In addition, when $n = 1.5$ the in-plane normal stress $\sigma_{xx}^{**}(z)$ and the in-plane shear stress $\sigma_{xy}^{**}(z)$ have the value of zero at $z/h \approx 0.1481$. The transverse shear stress $\sigma_{xz}^{**}(z)$ obtains the maximum value at $z/h \approx 0.220$.

Figure 6 shows the dimensionless deflection w^{**} of the full clamped FG nanoplates resting on the elastic foundation under sinusoidally distributed load. The influences of length-to-thickness ratio a/h and the volume-fraction exponent n on the deflection of nanoplates are examined. It is observed that the dimensionless deflections w^{**} decreases rapidly when the length-to-thickness ratio a/h increases from 5 to 10. However, they decrease slowly in the case of variation from 10 to 20. Figure 6b, Fig. 6c and Fig. 6d depict the in-plane normal stress $\sigma_{xx}^{**}(z)$, the in-plane shear stress $\sigma_{xy}^{**}(z)$ and the transverse shear stress $\sigma_{xz}^{**}(z)$ at points on the vertical line passing through the centroid of FG nanoplates with the length-to-thickness ratio $a/h = 10$.

Figure 7a shows the dimensionless deflection w^{**} of the simply supported FG nanoplates resting on the elastic

Table 7 The dimensionless deflection and maximum in-plane normal stress of the FG nanoplates resting on the elastic foundation versus to the variation of the volume-fraction exponent and nonlocal coefficient under the uniform distributed load

μ	w^{**}				$\sigma_{xx}^{**}(h/2)$			
	$n = 0.5$	1	4	10	0.5	1	4	10
$(K_w, K_s) = (0, 0)$								
0	7.1411	9.2661	13.8486	15.8346	38.1813	44.9593	59.2262	74.1338
1	8.3159	10.7943	16.1059	18.3866	42.9244	50.5434	66.5773	83.3455
2	9.4907	12.3224	18.3632	20.9387	47.6675	56.1275	73.9283	92.5572
3	10.6656	13.8506	20.6205	23.4908	52.4107	61.7116	81.2794	101.7689
4	11.8404	15.3788	22.8778	26.0429	57.1538	67.2957	88.6304	110.9806
$(K_w, K_s) = (100, 0)$								
0	4.9940	5.9428	7.5130	8.0404	25.7073	27.4403	29.8329	34.6241
1	5.4597	6.4188	7.9314	8.4129	26.4906	27.7219	29.1234	33.4454
2	5.8693	6.8261	8.2713	8.7096	27.0396	27.7772	28.2900	32.2001
3	6.2315	7.1773	8.5508	8.9494	27.3997	27.6623	27.3891	30.9414
4	6.5536	7.4822	8.7833	9.1456	27.6069	27.4193	26.4580	29.7014
$(K_w, K_s) = (0, 10)$								
0	3.8703	4.4146	5.2201	5.4676	19.6997	20.1422	20.5716	23.4724
1	4.3028	4.8783	5.7092	5.9579	20.9512	21.2569	21.5431	24.5809
2	4.7141	5.3192	6.1789	6.4322	22.2310	22.4333	22.6230	25.8213
3	5.1048	5.7371	6.6248	6.8836	23.5189	23.6407	23.7711	27.1516
4	5.4760	6.1329	7.0465	7.3110	24.8013	24.8578	24.9539	28.5296
$(K_w, K_s) = (100, 10)$								
0	3.1242	3.4640	3.9246	4.0547	15.3978	15.1806	14.6496	16.4282
1	3.3651	3.6992	4.1367	4.2562	15.6241	15.2058	14.4941	16.2612
2	3.5823	3.9113	4.3313	4.4433	15.8854	15.3133	14.4762	16.2556
3	3.7783	4.1020	4.5071	4.6133	16.1621	15.4683	14.5480	16.3617
4	3.9558	4.2738	4.6654	4.7666	16.4424	15.6493	14.6747	16.5369

foundation under sinusoidal distributed load versus to the variations of the foundation stiffness and the length-to-thickness ratio a/h. Figure 7b, Fig. 7c and Fig. 7d illustrate the in-plane normal stress $\sigma_{xx}^{**}(z)$, the in- plane shear stress $\sigma_{xy}^{**}(z)$ and the transverse shear stress $\sigma_{xz}^{**}(z)$ at points on the vertical line passing through the centroid of FG nanoplates versus to the variation of the foundation stiffness. It is clear seen that when the volume-fraction exponent n is constant, the transverse shear stress $\sigma_{xz}^{**}(z)$ has the same shape and different value.

Figure 8 show the dimensionless deflection w^{**} and the in-plane normal stress $\sigma_{xx}^{**}(h/2)$ of the FG nanoplates $(n = 1.5, \mu = 1, a/h = 10)$ resting on the elastic foundation under sinusoidally distributed load versus to the variations of the foundation stiffness, the volume-fraction exponent n and the boundary conditions. From Fig. 8c and Fig. 8d, it can be found that the displacements of FG plates decrease linearly with the increase of the parameter K_w but decrease nonlinear with the increase of the parameter K_s.

3.3 Free vibration problem

This sub-section considers the influences of the elastic foundations, the nonlocal coefficient, the volume-fraction exponent, the geometric parameters and the boundary conditions versus to the free vibration of the FG nanoplates.

Table 11 presents the effects of the various boundary conditions *and* the variation of the volume-fraction exponent and the nonlocal coefficient versus to the dimensionless fundamental frequency Ω^* of the FG nanoplates $(a/h = 10)$ resting on elastic foundation. It is seen that the dimensionless fundamental frequency Ω^* decreases gradually via the following order of boundary conditions: CCCC, CCCS, CSCS, CSSS, CFCF, SSSS, CSFS, SFSS. It is also found that the

Table 8 The dimensionless deflection and maximum in-plane normal stress of the FG nanoplates resting on the elastic foundation versus to the variation of the volume-fraction exponent and nonlocal coefficient under the sinusoidal distributed load

μ	w^{**}				$\sigma_{xx}^{**}(h/2)$			
	$n = 0.5$	1	4	10	0.5	1	4	10
$(K_w, K_s) = (0, 0)$								
0	4.5398	5.8891	8.8131	10.0899	26.5902	31.3156	41.3178	51.7205
1	5.4359	7.0516	10.5527	12.0815	31.8389	37.4971	49.4736	61.9298
2	6.3321	8.2140	12.2923	14.0732	37.0876	43.6785	57.6294	72.1390
3	7.2282	9.3765	14.0320	16.0648	42.3363	49.8600	65.7853	82.3482
4	8.1243	10.5389	15.7716	18.0565	47.5850	56.0415	73.9411	92.5574
$(K_w, K_s) = (100, 0)$								
0	3.2091	3.8292	4.8828	5.2514	18.8047	20.3746	22.9167	26.9510
1	3.6322	4.2886	5.3729	5.7434	21.2845	22.8203	25.2200	29.4792
2	4.0113	4.6922	5.7896	6.1569	23.5070	24.9692	27.1789	31.6056
3	4.3530	5.0496	6.1481	6.5094	25.5104	26.8726	28.8657	33.4193
4	4.6625	5.3682	6.4599	6.8134	27.3257	28.5702	30.3336	34.9848
$(K_w, K_s) = (0, 10)$								
0	2.4952	2.8545	3.4014	3.5761	14.6208	15.1892	15.9679	18.3563
1	2.8642	3.2584	3.8503	4.0373	16.7636	17.3135	18.0286	20.6617
2	3.2104	3.6360	4.2700	4.4694	18.7798	19.3064	19.9734	22.8479
3	3.5370	3.9913	4.6645	4.8758	20.6838	21.1854	21.8117	24.9191
4	3.8465	4.3271	5.0370	5.2597	22.4924	22.9692	23.5621	26.8955
$(K_w, K_s) = (100, 10)$								
0	2.0319	2.2639	2.5947	2.6952	11.9120	12.0545	12.1953	13.8528
1	2.2699	2.5106	2.8478	2.9489	13.2876	13.3423	13.3373	15.0934
2	2.4818	2.7286	3.0703	3.1720	14.5175	14.4870	14.3587	16.2095
3	2.6722	2.9232	3.2678	3.3698	15.6226	15.5097	15.2681	17.2035
4	2.8446	3.0984	3.4446	3.5467	16.6240	16.4325	16.0862	18.0978

Table 9 The variation of the dimensionless deflection of the FG nanoplates resting on the elastic foundation under the sinusoidal distributed load versus to the variation of the boundary condition, the nonlocal coefficient μ and the volume-fraction exponent n

n	μ	Boundary condition							
		CCCC	CCCS	CSCS	CSSS	SSSS	CFCF	CCFF	CFFF
0	0	0.9103	1.0384	1.1794	1.4839	1.8797	1.4922	5.4828	9.6907
	1	1.0407	1.2008	1.3791	1.7255	2.1721	1.7337	6.3688	11.5200
	2	1.1611	1.3540	1.5710	1.9555	2.4474	1.9826	7.2131	13.3259
	3	1.2727	1.4989	1.7559	2.1751	2.7077	2.2492	8.0205	15.1091
	4	1.3767	1.6364	1.9344	2.3854	2.9548	2.5136	8.7948	16.8754
1	0	1.4950	1.6761	1.8728	2.2580	2.7284	2.3059	6.5874	11.0759
	1	1.6622	1.8997	2.1617	2.5890	3.1061	2.7277	7.5653	13.1525
	2	1.8114	2.1056	2.4354	2.8995	3.4567	3.1453	8.4879	15.2012
	3	1.9455	2.2962	2.6958	3.1922	3.7842	3.5586	9.3630	17.2333
	4	2.0668	2.4737	2.9444	3.4696	4.0918	3.9681	10.1968	19.2463
4	0	1.9684	2.1657	2.3781	2.7705	3.2344	2.9653	7.1214	11.8054
	1	2.1398	2.4157	2.7186	3.1475	3.6505	3.4960	8.1116	14.0098
	2	2.2918	2.6448	3.0398	3.5002	4.0361	4.0222	9.0452	16.1870
	3	2.4267	2.8552	3.3441	3.8316	4.3955	4.5433	9.9293	18.3564
	4	2.5474	3.0496	3.6334	4.1445	4.7324	5.0591	10.7704	20.4976
10	0	2.1758	2.3739	2.5866	2.9712	3.4216	3.2472	7.3029	12.0760
	1	2.3414	2.6294	2.9450	3.3636	3.8497	3.8230	8.2873	14.3275
	2	2.4901	2.8644	3.2834	3.7308	4.2468	4.3948	9.2186	16.5558
	3	2.6218	3.0801	3.6037	4.0759	4.6172	4.9610	10.1010	18.7739
	4	2.7394	3.2790	3.9079	4.4015	4.9642	5.5215	10.9785	20.9630

Table 10 The variation of the dimensionless deflection of the FG nanoplates resting on the elastic foundation versus to the variation of the boundary condition, the nonlocal coefficient μ and the length-to-thickness ratio a/h

μ	a/h	Boundary condition						
		CCCC	CCCS	CSCS	CSSS	SSSS	CFSS	SFSS
1	5	1.9508	2.1595	2.3898	2.7217	3.1185	3.7133	4.2109
	10	1.6784	1.9054	2.1545	2.5347	2.9838	3.5912	4.1085
	25	1.5879	1.8212	2.0770	2.4635	2.9161	3.4964	4.0060
	1000	1.5811	1.8149	2.0713	2.4514	2.8951	3.4549	3.9544
	10000	1.5811	1.8149	2.0712	2.4513	2.8951	3.4548	3.9543
2	5	2.0911	2.3600	2.6607	3.0164	3.4385	4.0746	4.7716
	10	1.8191	2.0997	2.4125	2.8204	3.2986	3.9499	4.6590
	25	1.7274	2.0121	2.3292	2.7446	3.2275	3.8489	4.5458
	1000	1.7205	2.0055	2.3229	2.7317	3.2056	3.8043	4.4889
	10000	1.7205	2.0055	2.3229	2.7317	3.2055	3.8042	4.4887
3	5	2.2158	2.5435	2.9152	3.2911	3.7341	4.4083	5.3051
	10	1.9443	2.2778	2.6552	3.0868	3.5892	4.2806	5.1831
	25	1.8518	2.1873	2.5666	3.0068	3.5152	4.1741	5.0603
	1000	1.8448	2.1804	2.5599	2.9934	3.4925	4.1271	4.9985
	10000	1.8448	2.1804	2.5599	2.9933	3.4924	4.1269	4.9983
4	5	2.3270	2.7124	3.1555	3.5484	4.0088	4.7173	5.8134
	10	2.0566	2.4421	2.8846	3.3363	3.8591	4.5867	5.6828
	25	1.9637	2.3490	2.7911	3.2527	3.7824	4.4756	5.5513
	1000	1.9566	2.3419	2.7840	3.2387	3.7591	4.4266	5.4852
	10000	1.9566	2.3419	2.7840	3.2386	3.7590	4.4264	5.4850

increase of the nonlocal coefficient makes the FG nanoplates become softer, and hence makes the dimensionless fundamental frequency decrease. These results again help fill in the gap of those that the analytical method is missing.

Figure 9a illustrates the variation of the dimensionless fundamental frequency of the FG nanoplates with the volume-fraction exponents $n = 2$ resting on the elastic foundation versus to the variation of the length-to-thickness a/h. It can be seen that the dimensionless fundamental frequency of the FG nanoplates decreases rapidly when the length-to-thickness ratio a/h varies from 5 to 15. However, they decrease slowly when the length-to-thickness ratio a/h varies from 20 to 50. Figure 9b demonstrates the effect of the volume-fraction exponents n and the nonlocal coefficient on the variation of the dimensionless fundamental frequency of the FG nanoplates resting on the elastic foundation. It is seen that the dimensionless fundamental frequency decreases rapidly when the volume-fraction exponent varies from 0 to 2, but decreases slowly when the volume-fraction exponent varies from 2 to 10.

Figure 10 demonstrates the variation of the fundamental frequency Ω^* of the FG nanoplates resting on the elastic foundation$(n = 1, \mu = 1, CCCC)$ with different foundation parameters versus to the variations of width-to-length b/a and of the volume-fraction exponents n $(a/h = 20)$ and of the length-to-thickness$a/h, (b/a = 1)$. Figure 11 shows the variation of the dimensionless fundamental frequency of the FG nanoplates resting on the elastic foundation $(\mu = 1, K_{w1} = 10, K_{s1} = 10)$ in the various boundary conditions versus to the variations of the length-to-thickness a/h $(n = 1)$ and of the volume-fraction exponent n $(h = 10)$. Figure 12 presents the variation of the dimensionless fundamental frequency of the FG nanoplates resting on the elastic foundation $(n = 1.5, a/h = 10, CCCC)$ with different nonlocal coefficients versus to the variations of the elastic foundation coefficient$K_{w1}, (K_{s1} = 10)$ and of $K_{s1}, \left(K_{w1} = 50\right)$. The results from these figures show that the increase of the width-to-length ratio makes the nanoplates become softer and thus makes the fundamental frequency Ω^* decrease. Furthermore, the increase of the elastic foundation stiffness

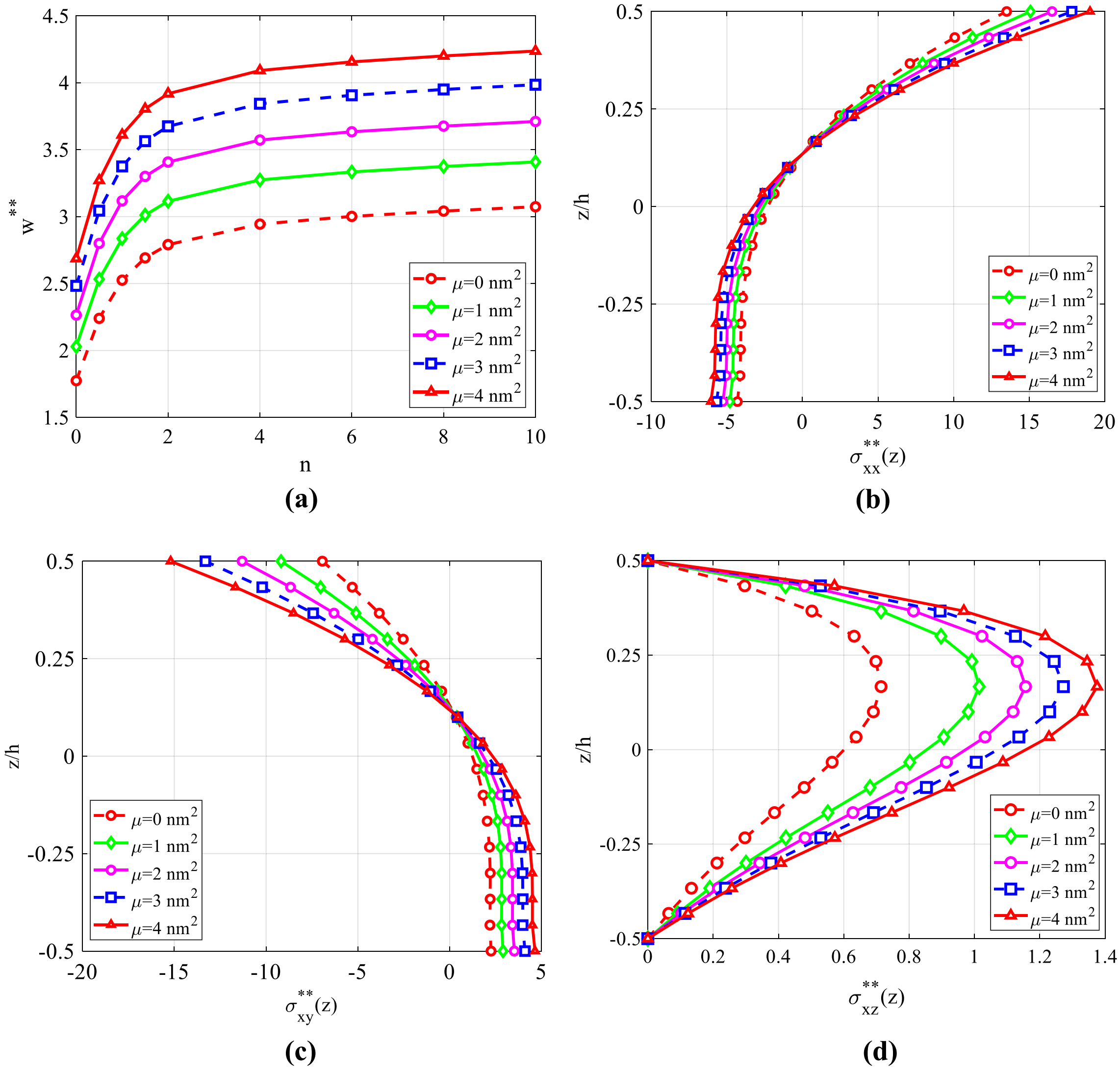

Fig. 5 The effect of nonlocal coefficient μ and n versus to (**a**) *tothedimensionlessdeflection*, **b** to the in-plane normal stress $\sigma_{xx}^{**}(z)$; **c** to the in-plane shear stress $\sigma_{xy}^{**}(z)$; **d** to the transverse shear stress $\sigma_{xz}^{**}(z)$ of FG nanoplates resting on elastic foundations ($K_w = 10, K_s = 10, a/h = 10, n = 1.5, SSSS$)

leads to the increase of the fundamental frequency. Form Fig. 12, it can be seen that the fundamental frequency Ω^* depends linearly on the elastic foundation coefficient K_{w1} but depends nonlinearly on the elastic foundation coefficient K_{s1}.

Figure 13 shows the variations of the first six fundamental frequencies $10\omega_i h\sqrt{\frac{\rho_m}{E_m}}(i = 1/6)$ of the FG nanoplates versus to the variations of the nonlocal parameter μ, volume-fraction exponent n and elastic foundation coefficient K_{w1}. It can be seen that the increase of the nonlocal parameter and the volume-fraction exponent n leads to the decrease of all fundamental frequencies in which the mode (3,2) and mode (3,3) have the largest decrease. For example, the value of the fundamental frequency of the FG nanoplates of the mode (3,3) decreases more than 2.5 times, from 6.02 (with nonlocal parameter $\mu = 0$) to 2.365 (with nonlocal parameter $\mu = 4$). The volume-fraction exponent n has a significant influence on the fundamental frequency of the FG

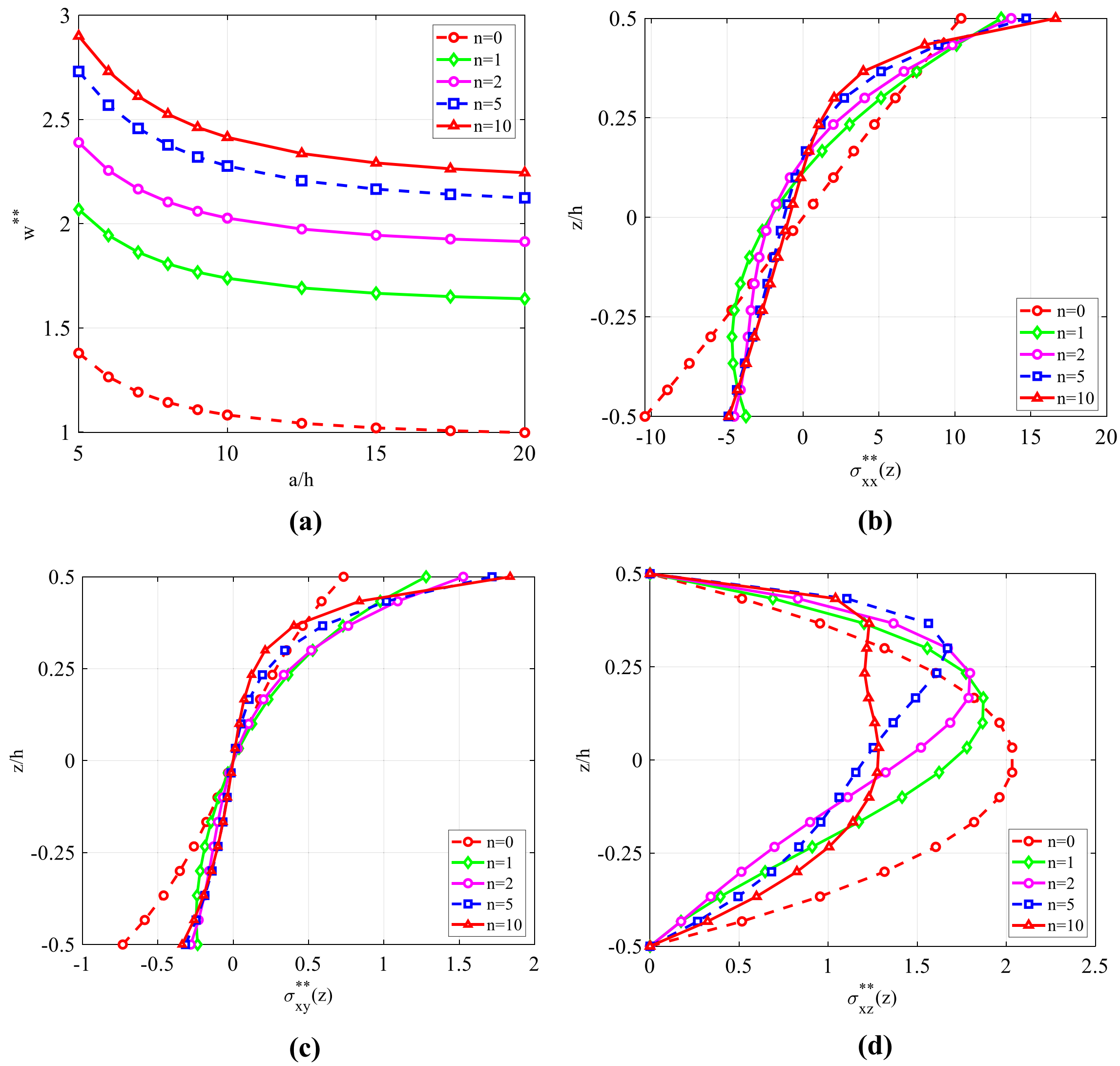

Fig. 6 The effects of length-to-thickness ratio a/h and the volume-fraction exponent n versus to: **a** the dimensionless deflection; **b** the in-plane normal stress $\sigma_{xx}^{**}(z)$; **c** the in-plane shear stress $\sigma_{xy}^{**}(z)$; **d** the transverse shear stress $\sigma_{xz}^{**}(z)$ of FG nanoplates resting on elastic foundations ($K_w = 10, K_s = 10, a/h = 10, \mu = 1, CCCC$)

nanoplates when n changes from 0 to 2 and the value of the modes decreases negligibly with $n \geq 2$. Figure 14 shows the nine mode shapes of the FG nanoplates resting on the elastic foundation. It can be found that the nanoplates resting on the elastic foundation still have the same shapes as the nanoplates without the elastic foundation.

4 Conclusions

A finite element formulation using four-unknown shear deformation theory is developed for bending and free vibration analysis of the FG nanoplates resting on the elastic medium foundation. In this formulation, a four-node quadrilateral element with eight degrees of freedom per

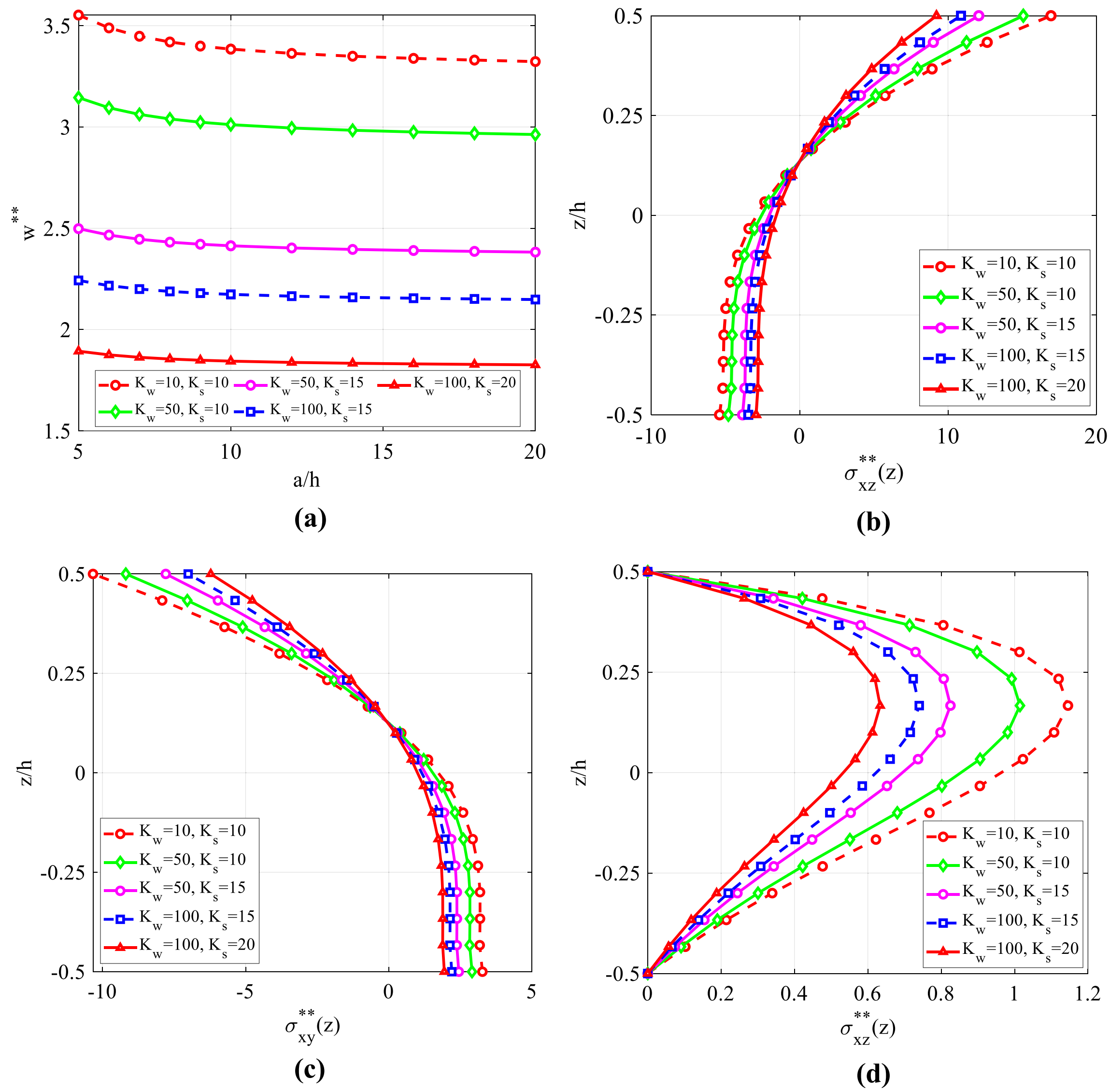

Fig. 7 The effect of length-to-thickness ratio a/h and the foundation stiffness K_w, K_s versus to: **a** the dimensionless deflection; **b** the in-plane normal stress $\sigma_{xx}^{**}(z)$; **c** the in-plane shear stress $\sigma_{xy}^{**}(z)$; **d** the transverse shear stress $\sigma_{xz}^{**}(z)$ of FG nanoplates resting on elastic foundations ($n = 1.5, \mu = 1$)

node and the four-unknown variables are approximated by Lagrangian and Hermitian interpolation functions to form the finite element formulation of the stiffness matrices, the mass matrices and the load vectors of the FG nanoplates with the second derivatives. Therefore, it is clear that this element is the most suitable for investigating the bending and free vibration responses of the FG nanoplates resting on the elastic medium foundation. The accuracy and the reliability of the present method have been validated by comparing its numerical results to those available in the literature. In addition, the analyses of the effects of various parameters on the bending and the free vibration of the FG nanoplates resting on the elastic foundation have been examined. It is thus very promising to extend the present

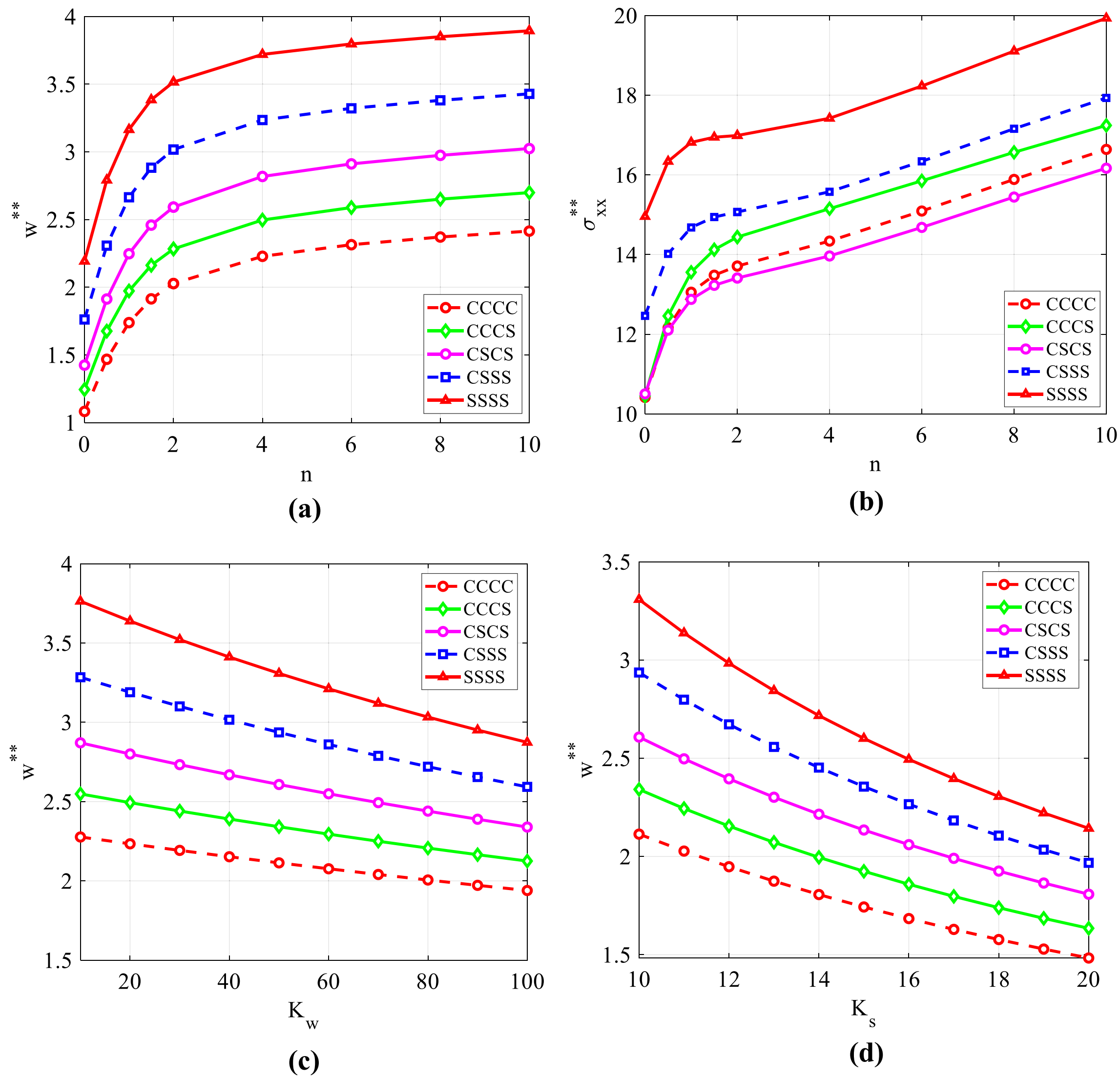

Fig. 8 The effect of the volume-fraction exponent n and the boundary conditions on: **a** the dimensionless deflection; **b** the in-plane normal stress $(h/2)(K_w = 10, K_s = 10)$

method for the analysis of the FG porous nanoplates with laws of variable thickness resting on elastic foundation, the FG porous plate resting on elastic foundation subjected to other loads, and the FG porous nanoshells resting on the elastic foundation. It is noted that the proposed method also exists a limit regarding using high-order shape functions to approximate displacement fields of the FG nanoplates. This limit in somehow leads to a rather high computation cost and hence should be a topic for improvement in coming studies.

Acknowledgements This research is funded by Vietnam National Foundation for Science and Technology Development (NAFOSTED) under Grant number 107.02–2019.330.

Table 11 The effect of the boundary condition, the nonlocal coefficient μ and the volume-fraction exponent n ($a/h = 10, K_{w1} = 50, K_{s1} = 50$) on the dimensionless fundamental frequency of the FG nanoplates resting on the elastic foundation. ·

n	μ	Boundary condition							
		CCCC	CCCS	CSCS	CSSS	CFCF	SSSS	CSFS	SFSS
0	0	10.8638	9.9443	9.2609	8.0486	7.0970	7.1115	5.1263	4.8631
	1	9.9892	9.1109	8.4792	7.4206	6.7025	6.6109	4.8672	4.6148
	2	9.3335	8.4820	7.8846	6.9396	6.3662	6.2236	4.6495	4.4054
	3	8.8210	7.9873	7.4134	6.5566	6.0757	5.9127	4.4637	4.2260
	4	8.4073	7.5856	7.0283	6.2424	5.8217	5.6561	4.3031	4.0703
0.5	0	9.6900	8.9267	8.3359	7.3379	6.3883	6.5680	4.8465	4.6273
	1	8.9836	8.2258	7.6607	6.7951	6.0359	6.1343	4.6149	4.3982
	2	8.4520	7.6949	7.1460	6.3784	5.7355	5.7977	4.4198	4.2048
	3	8.0350	7.2759	6.7373	6.0456	5.4760	5.5266	4.2529	4.0391
	4	7.6971	6.9346	6.4025	5.7719	5.2491	5.3023	4.1083	3.8951
1	0	9.0611	8.3973	7.8542	6.9779	6.0173	6.3008	4.7156	4.5208
	1	8.4508	7.7695	7.2361	6.4801	5.6869	5.9019	4.4985	4.3009
	2	7.9884	7.2916	6.7637	6.0966	5.4054	5.5909	4.3148	4.1152
	3	7.6238	6.9127	6.3876	5.7895	5.1622	5.3397	4.1573	3.9559
	4	7.3265	6.6028	6.0788	5.5362	4.9496	5.1311	4.0207	3.8174
4	0	8.2622	7.7550	7.3076	6.6181	5.5740	6.0730	4.6376	4.4759
	1	7.8097	7.2399	6.7687	6.1767	5.2754	5.7137	4.4369	4.2637
	2	7.4513	6.8370	6.3511	5.8324	5.0202	5.4304	4.2654	4.0840
	3	7.1611	6.5122	6.0155	5.5542	4.7993	5.1994	4.1176	3.9297
	4	6.9192	6.2431	5.7380	5.3232	4.6059	5.0064	3.9888	3.7954
10	0	8.0327	7.5671	7.1735	6.5507	5.4523	6.0497	4.6458	4.4947
	1	7.6433	7.0953	6.6621	6.1263	5.1658	5.7003	4.4496	4.2834
	2	7.3224	6.7186	6.2620	5.7926	4.9203	5.4230	4.2810	4.1043
	3	7.0576	6.4119	5.9386	5.5217	4.7074	5.1961	4.1352	3.9504
	4	6.8337	6.1558	5.6700	5.2960	4.5207	5.0059	4.0080	3.8164

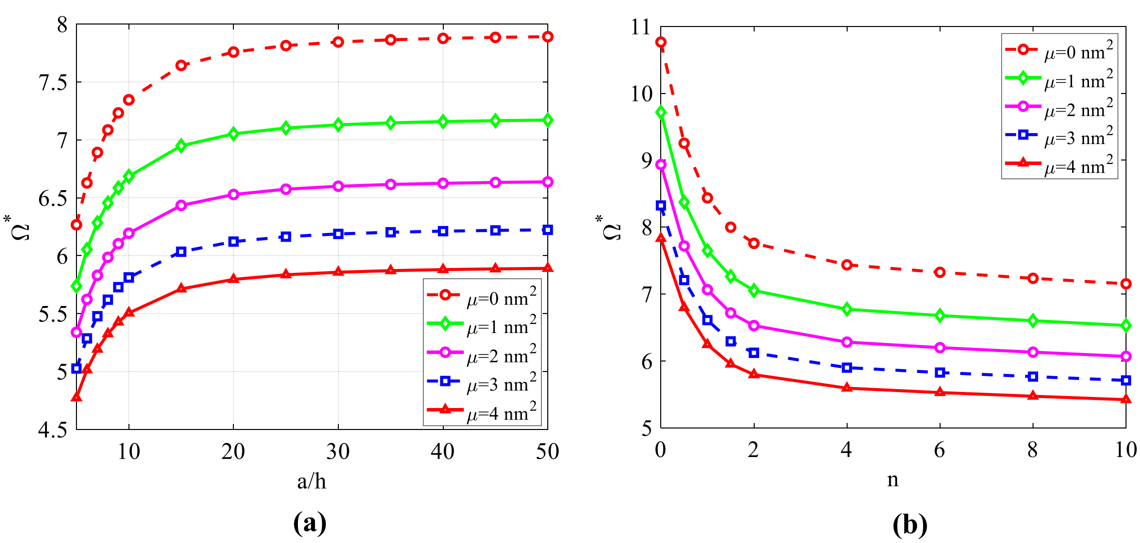

Fig. 9 The variation of the dimensionless fundamental frequency of the FG nanoplates resting on the elastic foundation ($K_{w1} = 50, K_{s1} = 10, CCCC$) with the various nonlocal coefficient versus to the variation of **a** the length-to-thickness a/h ($n = 2$); **b** the volume-fraction exponents n ($a/h = 20$)

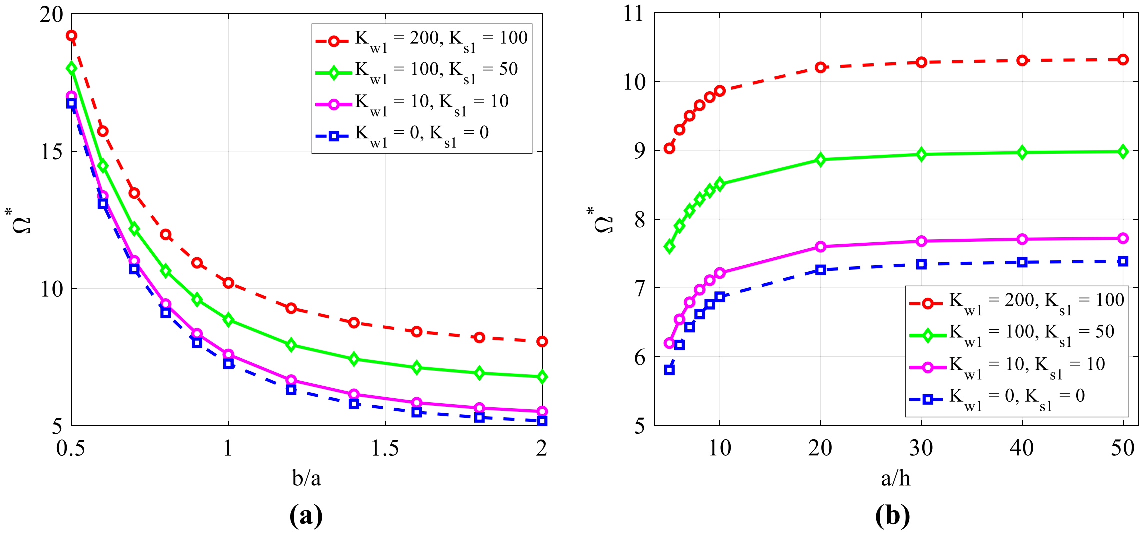

Fig. 10 The variation of the dimensionless fundamental frequency of the FG nanoplates resting on the elastic foundation $(n = 1, \mu = 1, CCCC)$ with different foundation parameters versus to the variation of: **a** the width-to-length ratio $b/a, (a/h = 20)$; **b** the length-to-thickness $a/h, (b/a = 1)$

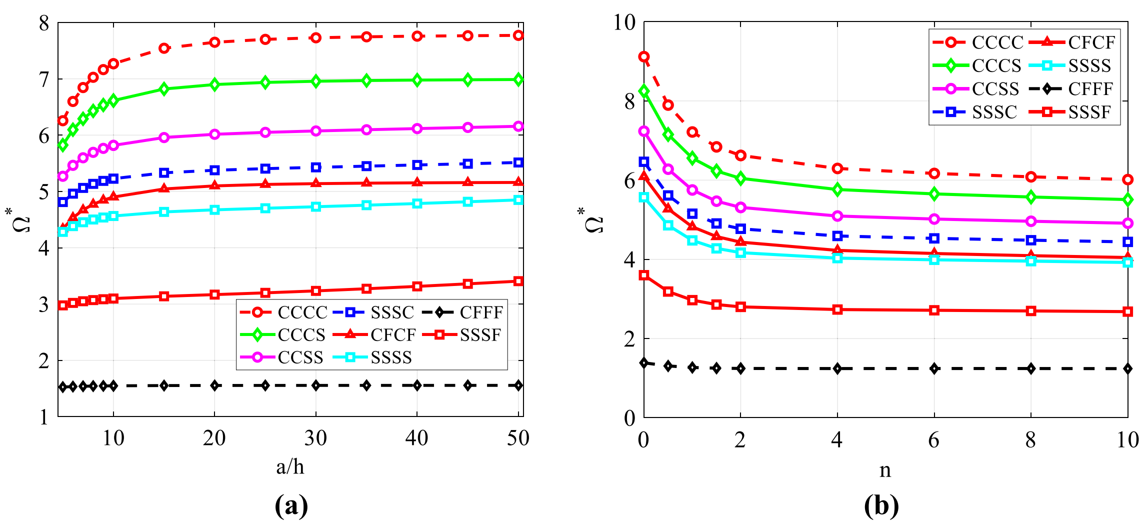

Fig. 11 The variation of the dimensionless fundamental frequency of the FG nanoplates resting on the elastic foundation $(\mu = 1, K_{w1} = 10, K_{s1} = 10)$ in the various boundary conditions versus to the variations of: **a** the length-to-thickness a/h $(n = 1)$; **b** the volume-fraction exponent n $(h = 10)$

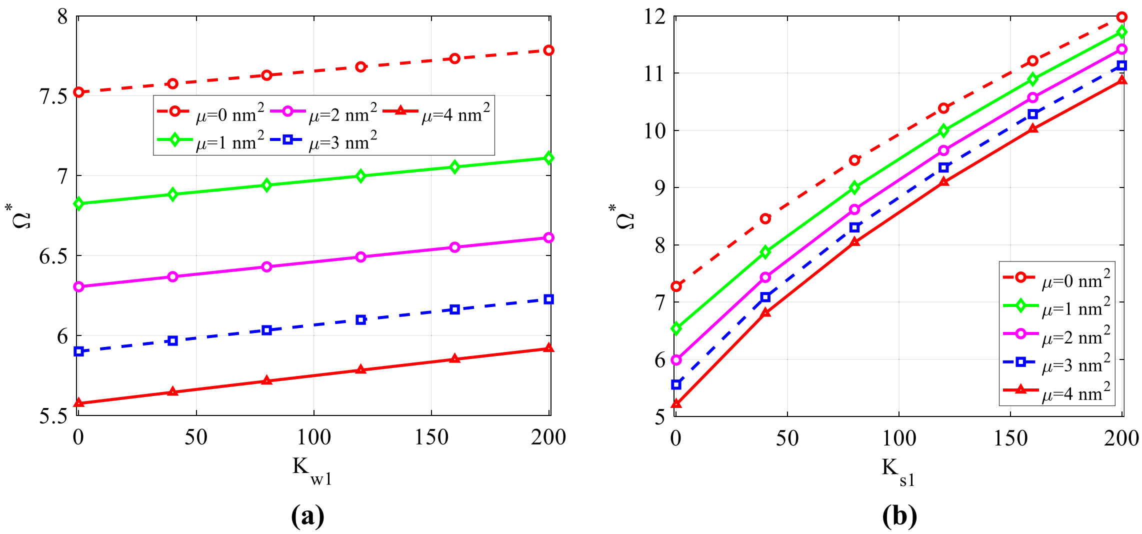

Fig. 12 The variation of the dimensionless fundamental frequency of the FG nanoplates resting on the elastic foundation $(n = 1.5, a/h = 10, CCCC)$ with different nonlocal coefficients versus to the variations of: **a** the elastic foundation coefficient K_{w1}, $(K_{s1} = 10)$; and **b** $K_{s1}, \left(K_{w1} = 50\right)$

Appendix A

$$\lambda_1 = \frac{1}{4}(1-\chi)(1-\zeta);\lambda_2 = \frac{1}{4}(1+\chi)(1-\zeta);$$

$$\lambda_3 = \frac{1}{4}(1+\chi)(1+\zeta);\lambda_4 = \frac{1}{4}(1-\chi)(1+\zeta);$$

$$\hbar_1 = \frac{1}{8}(1-\chi)(1-\zeta)\left(2-\chi-\zeta-\chi^2-\zeta^2\right);$$

$$\hbar_2 = \frac{1}{8}(1-\chi)(1-\zeta)\left(1-\chi^2\right)$$

$$\hbar_3 = \frac{1}{8}(1-\chi)(1-\zeta)\left(1-\zeta^2\right)$$

$$\hbar_4 = \frac{1}{8}(1+\chi)(1-\zeta)\left(2+\chi-\zeta-\chi^2-\zeta^2\right);$$

$$\hbar_5 = -\frac{1}{8}(1+\chi)(1-\zeta)\left(1-\chi^2\right)$$

$$\hbar_6 = \frac{1}{8}(1+\chi)(1-\zeta)\left(1-\zeta^2\right)$$

$$\hbar_7 = \frac{1}{8}(1+\chi)(1+\zeta)\left(2+\chi+\zeta-\chi^2-\zeta^2\right);$$

$$\hbar_8 = -\frac{1}{8}(1+\chi)(1+\zeta)\left(1-\chi^2\right);$$

$$\hbar_9 = -\frac{1}{8}(1+\chi)(1+\zeta)\left(1-\zeta^2\right);$$

$$\hbar_{10} = \frac{1}{8}(1-\chi)(1+\zeta)\left(2-\chi+\zeta-\chi^2-\zeta^2\right);$$

$$\hbar_{11} = \frac{1}{8}(1-\chi)(1+\zeta)\left(1-\chi^2\right);$$

$$\hbar_{12} = -\frac{1}{8}(1-\chi)(1+\zeta)\left(1-\zeta^2\right).$$

($\chi;\zeta$: are natural coordinates)

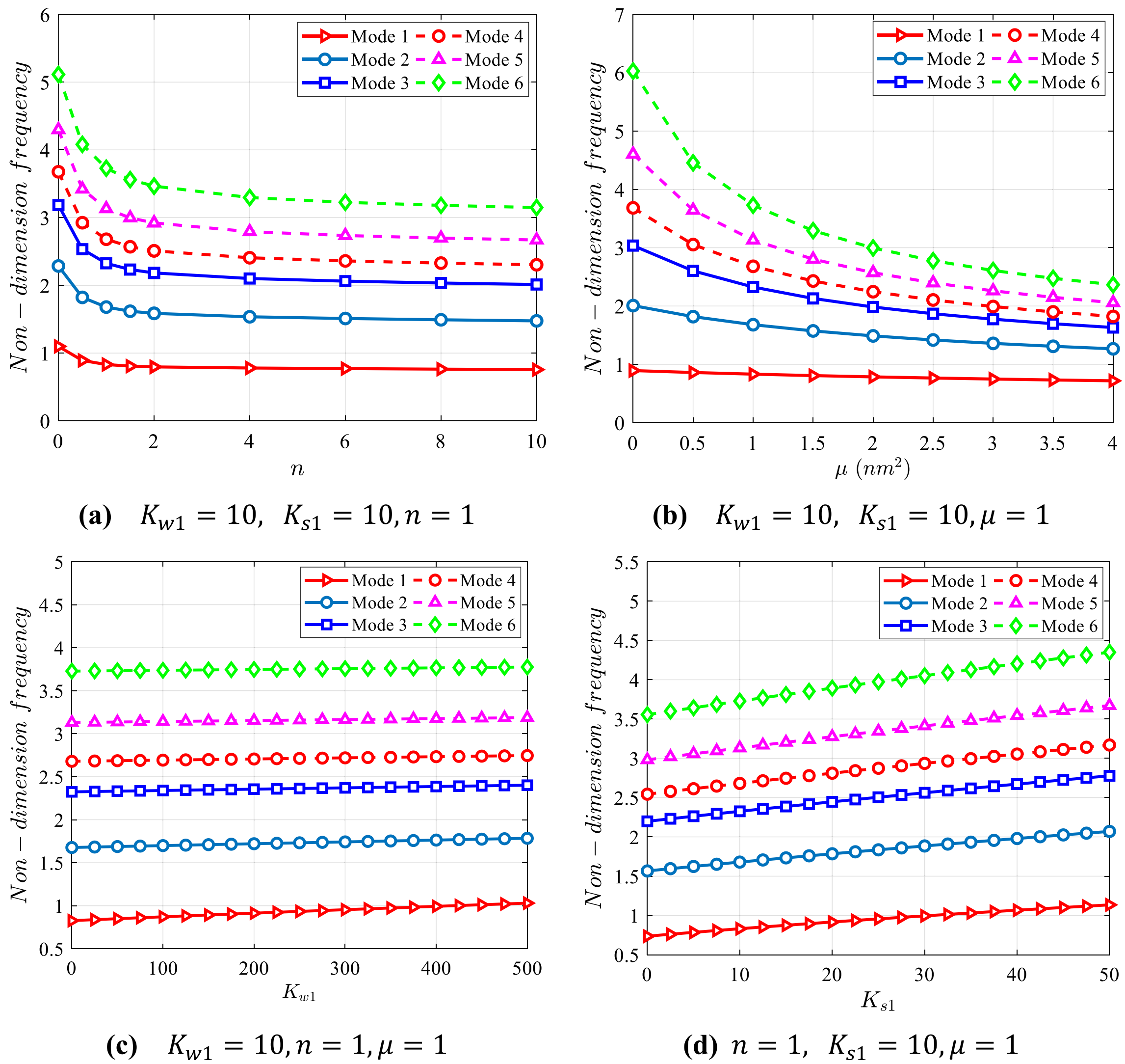

Fig. 13 The variations of the first six fundamental frequencies of the FG nanoplates ($a/h = 10, SSSS$) versus to the variations of: **a** the nonlocal parameter μ; **b** the volume-fraction exponent n; **c** the elastic foundation coefficient K_{w1}; **d** the elastic foundation coefficient K_{s1}

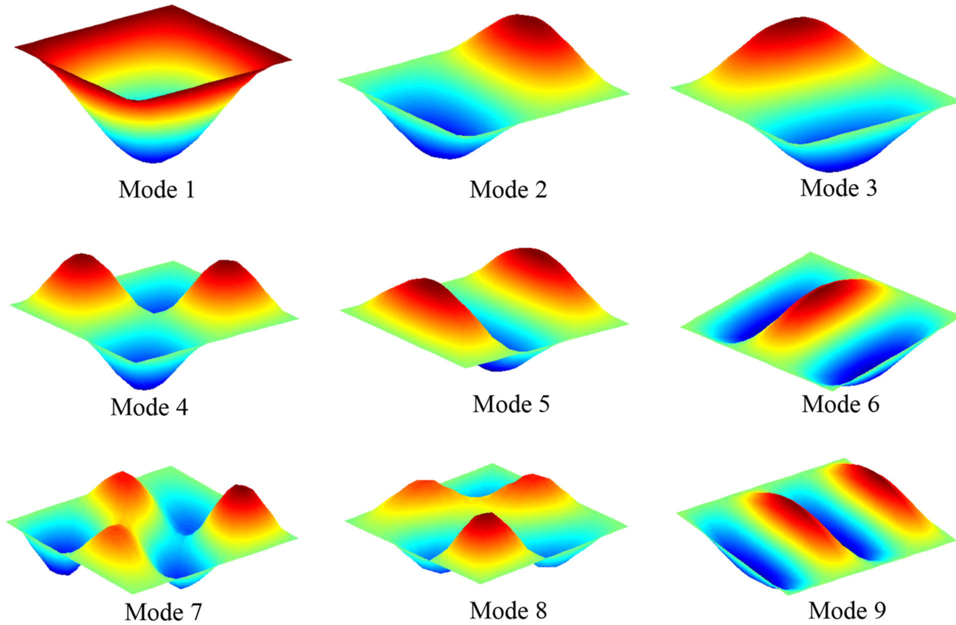

Fig. 14 The first nine mode shapes of FG nanoplates resting on the elastic foundation

Appendix B

$$B_1 = \begin{bmatrix} N_{u,x} \\ N_{v,y} \\ N_{u,y} + N_{v,x} \end{bmatrix}; B_2 = -\begin{bmatrix} N_{wb,xx} \\ N_{wb,yy} \\ 2N_{wb,xy} \end{bmatrix}; B_3 = -\begin{bmatrix} N_{ws,xx} \\ N_{ws,yy} \\ 2N_{ws,xy} \end{bmatrix}; B_1^b = \begin{bmatrix} N_{ws,x} \\ N_{ws,y} \end{bmatrix};$$

$$B_{wx2} = \left[N_{wb,xx} + N_{ws,xx}\right]; B_{wy2} = \left[N_{wb,yy} + N_{ws,yy}\right];$$

$$B_{wx2} = \left[N_{wb,xx} + N_{ws,xx}\right]; B_{wy2} = \left[N_{wb,yy} + N_{ws,yy}\right]$$

$$\mathrm{N} = \left[N_u^T \; N_v^T \; N_{wb}^T \; N_{ws}^T \; N_{wb,x}^T \; N_{ws,x}^T \; N_{wb,y}^T \; N_{ws,y}^T \right]^T; \mathrm{N}_x = \frac{\partial N}{\partial x}; \mathrm{N}_y = \frac{\partial N}{\partial y}$$

$$D_m = \begin{bmatrix} I_0 & 0 & 0 & 0 & I_1 & J_1 & 0 & 0 \\ & I_0 & 0 & 0 & 0 & 0 & I_1 & J_0 \\ & & I_0 & 0 & 0 & 0 & 0 & 0 \\ & & & I_0 & 0 & 0 & 0 & 0 \\ & & & & I_2 & J_2 & 0 & 0 \\ & & & & & K_2 & 0 & 0 \\ & & & & & & I_2 & J_2 \\ sym & & & & & & & K_2 \end{bmatrix}$$

References

1. Wang Q, Varadan V (2006) Wave characteristics of carbon nanotubes. Int J Solids Struct 43(2):254–265
2. Nicolas GH, Anthony TP (1997) Heterogeneous atomistic-continuum representations for dense fluid systems. Int J Mod Phys C 8(4):967–976
3. Eringen AC (1983) On differential equations of nonlocal elasticity and solutions of screw dislocation and surface waves. J Appl Phy 54:4703–4710
4. Eringen AC (2002) Nonlocal continuum field theories. Springer, New York
5. Ansari R, Sahmani S, Arash B (2010) Nonlocal plate model for free vibrations of single-layered graphene sheets. Phys Lett A 375(1):53–62
6. Arash B, Wang Q (2012) A review on the application of nonlocal elastic models in modeling of carbon nanotubes and graphenes. Comput Mater Sci 51(1):303–313
7. Asemi SR, Farajpour A (2014) Decoupling the nonlocal elasticity equations for thermomechanical vibration of circular graphene sheets including surface effects. Phys E 60:80–90
8. Jalali SK, Jomehzadeh E, Pugno NM (2016) Influence of out-of-plane defects on vibration analysis of graphene: molecular

dynamics and non-local elasticity approaches. Superlattice Microst 91:331–344
9. Ahababaei R, Reddy JN (2009) Nonlocal third-order shear deformation plate theory with application to bending and vibration of plate. J Sound Vib 326(1–2):277–289
10. Pradhan SC, Murmu T (2009) Small scale effect on the buckling of single-layered graphene sheets under biaxial compression via nonlocal continuum mechanics. Comput Mater Sci 47(1):268–274
11. Reddy JN (2010) Nonlocal nonlinear formulations for bending of classical and shear deformation theories of beams and plates. Int J Eng Sci 48(11):1507–1518
12. Prandhan SC, Phadikar JK (2011) Nonlocal theory for buckling of nanoplates. Int J Struct Stabil Dynam 11(3):411–429
13. Farajpour A, Danesh M, Mohammadi M (2011) Buckling analysis of variable thickness nanoplates using nonlocal continuum mechanics. Phys E 44(3):719–727
14. Murmu T, Adhikari S (2011) Nonlocal vibration of bonded double-nanoplate-systems. Compos B Eng 42(7):1901–1911
15. Aksencer T, Aydogdu M (2012) Forced transverse vibration of nanoplates using nonlocal elasticity. Phys E 44(7–8):1752–1759
16. Satish N, Narendar S, Gopalakrishnan S (2012) Thermal vibration analysis of orthotropic nanoplates based on nonlocal continuum mechanics. Phys E 44(9):1950–1962
17. Shen ZB, Tang HL, Li KK, Tang GJ (2012) Vibration of single-layered graphene sheet-based nanomechanical sensor via nonlocal Kirchhoff plate theory. Comput Mater Sci 61:200–205
18. Hashemi SH, Zare M, Nazemnezhad R (2013) An exact analytical approach for free vibration of Mindlin rectangular nano-plate via nonlocal elasticity. Compos Struct 100:290–299
19. Fazelzadeh SA, Ghavanloo E (2014) Nanoscale mass sensing based on vibration of single layered grapheme sheet in thermal environments. Acta Mech Sin 30(1):84–91
20. Ke LL, Wang YS, Yang J, Kitipornchai S (2014) Free vibration of size-dependent magneto-electro-elastic nanoplates based on the nonlocal theory. Acta Mech Sin 30(4):516–525
21. Malekzadeh P, Golbahar HMR, Shojaee M (2014) Nonlinear free vibration of skew nanoplates with surface and small scale effects. Thin Wall Struct 78:48–56
22. Craciunescu CM, Wuttig M (2014) New ferromagnetic and functionally graded shape memory alloys. J Optoelectron Adv Mat 5(1):139–146
23. Fu Y, Du H, Zhang S (2003) Functionally graded TiN/TiNi shape memory alloy films. J Mater Lett 57(20):2995–2999
24. Lee Z, Ophus C, Fischer LM, Fitzpatrick NN, Westra KL, Evoy S, Radmilovic V, Dahmen U, Mitlin D (2006) Metallic NEMS components fabricated from nanocomposite Al–Mo films. J Nanotechnol 17(12):3063–3070
25. Natarajan S, Chakraborty S, Thangavel M, Bordas S, Rabczuk T (2012) Size-dependent free flexural vibration behavior of functionally graded nanoplates. Comput Mater Sci 65:74–80
26. Jung WY, Han SC (2013) Analysis of sigmoid functionally graded material (S-FGM) nanoscale plates using the nonlocal elasticity theory. Math Probl Eng 49:449–458
27. Nami MR, Janghorban M, Damadam M (2015) Thermal buckling analysis of functional graded rectangular nanoplates based on nonlocal third-order shear deformation theory. Aerosp Sci Tech 41:7–15
28. Hashemi SH, Bedroud M, Nazemnezhad R (2013) An exact analytical solution for free vibration of functionally graded circular/annular Mindlin nanoplates via nonlocal elasticity. Compos Struct 103:108–118
29. Salehipour H, Nahvi H, Shahidi AS (2015) Exact analytical solution for free vibration of functionally graded micro/nanoplates via three-dimensional nonlocal elasticity. Phys E 66:350–358
30. Salehipour H, Shahidi AS, Nahvi H (2015) Modified nonlocal elasticity theory for functionally graded materials. Int J Eng Sci 90:44–57
31. Ansari R, Shojaei MF, Shahabodini A, Vahdati MB (2015) Three-dimensional bending and vibration analysis of functionally graded nanoplates by a novel differential quadrature-based approach. Compos Struct 131:753–764
32. Karimi M, Haddad HA, Shahidi AR (2015) Combining surface effects and non-local two variable refined plate theories on the shear/biaxial buckling and vibration of silver nanoplates. Micro Nano Lett 10(6):276–281
33. Karimi M, Shahidi AR (2017) Nonlocal, refined plate, and surface effects theories used to analyze free vibration of magneto-electro-elastic nanoplates under thermo-mechanical and shear loadings. Appl Phys A 123:304
34. Karimi M, Shahidi AR (2019) A general comparison the surface layer degree on the out-of phase and in-phase vibration behavior of a skew double-layer magneto–electro–thermo-elastic nanoplate. Appl Phys A 125:106
35. Karimi M, Shahidi AR (2019) Comparing magnitudes of surface energy stress in synchronous and asynchronous bending/buckling analysis of slanting double-layer METE nanoplates. Appl Phys A 125:154
36. Karimi M, Shahidi AR (2018) Buckling analysis of skew magneto-electro-thermo-elastic nanoplates considering surface energy layers and utilizing the Galerkin method. Appl Phys A 124:681
37. Farajpour MR, Shahidi AR, Farajpour A (2019) Influences of non-uniform initial stresses on vibration of small-scale sheets reinforced by shape memory alloy nanofibers. Eur Phys J Plus 134:218
38. Karimi M, Mirdamadi HR, Shahidi AR (2017) Positive and negative surface effects on the buckling and vibration of rectangular nanoplates under biaxial and shear in-plane loadings based on nonlocal elasticity theory. J Braz Soc Mech Sci Eng 39(4):1391–1404
39. Karimi M, Shokrani MH, Shahidi AR (2015) Size-dependent free vibration analysis of rectangular nanoplates with the consideration of surface effects using finite difference method. J Appl Comput Mech 1(3):122–133
40. Karimi M, Shahidi AR (2015) Finite difference method for sixth-order derivatives of differential equations in buckling of nanoplates due to coupled surface energy and non-local elasticity theories. Int J Nano Dimens 6(5):525–537
41. Karimi M, Shahidi AR (2016) Finite difference method for biaxial and uniaxial buckling of rectangular silver nanoplates resting on elastic foundations in thermal environments based on surface stress and nonlocal elasticity theories. J Solid Mech 8(4):719–733
42. Morteza K, Ali RS (2017) Thermo-mechanical vibration, buckling, and bending of orthotropic graphene sheets based on nonlocal two-variable refined plate theory using finite difference method considering surface energy effects. Proc IMechE Part N J Nanomater Nanoeng Nanos
43. Farajpour MR, Shahidi AR, Farajpour A (0850a) Elastic waves in fluid-conveying carbon nanotubes under magneto-hygro-mechanical loads via a two-phase local/nonlocal mixture mode. Mater Res Express 6:0850a8
44. Morteza K, Ali RS (2015) A comprehensive investigation into the impact of nonlocal strain gradient and modified couple stress models on the rates of surface energy layers of BiTiO3-CoFe2O4 nanoplates: A vibration analysis. Mater Res Express
45. Wang YZ, Li FM (2012) Static bending behaviors of nanoplate embedded in elastic matrix with small scale effects. Mech Res Comm 41:44–48
46. Narendar S, Gopalakrishnan S (2012) Nonlocal continuum mechanics based ultrasonic flexural wave dispersion

characteristics of a monolayer graphene embedded in polymer matrix. Compos B Eng 43:3096–3103
47. Pouresmaeeli S, Ghavanloo E, Fazelzadeh SA (2013) Vibration analysis of viscoelastic orthotropic nanoplates resting on viscoelastic medium. Compos Struct 96:405–410
48. Zenkour AM, Sobhy M (2013) Nonlocal elasticity theory for thermal buckling of nanoplates lying on Winkler-Pasternak elastic substrate medium. Phys E 53:251–259
49. Panyatong M, Chinnaboon B, Chucheepsakul S (2015) Incorporated effects of surface stress and nonlocal elasticity on bending analysis of nanoplates embedded in an elastic medium. Suranaree J Sci Technol 22(1):21–33
50. Shimpi RP (2002) Refined plate theory and its variants. AIAA J 40(1):137–146
51. Ismail M, Hassen AA, Abdlouahed T (2010) A two variable refined plate theory for the bending analysis of functionally graded plates. Acta Mech Sin 26(6):941–949
52. Abdelkader B, Hassaine DT, Hassen AA, Abdelouahed T, Meftah SA (2011) A four variable refined plate theory for free vibrations of functionally graded plates with arbitrary gradient. Compos B Eng 42(6):1386–1394
53. Thai-Huu T, Dong-Ho C (2013) Finite element formulation of various four unknown shear deformation theories for functionally graded plates. Finite Elem Anal Des 75:50–61
54. Sobhy M (2015) A comprehensive study on FGM nanoplates embedded in an elastic medium. Compos Struct 134:966–980
55. Thai-Huu T, Dong-Ho C (2011) A refined plate theory for functionally graded plates resting on elastic foundation. Compos Sci Technol 71(16):1850–1858
56. Thai-Huu T, Park T, Dong-Ho C (2013) An efficient shear deformation theory for vibration of functionally graded plates. Arch Appl Mech 83(1):137–149
57. Mohammed A, Abdelouahed T, Ismail M, Abbes AEB (2011) A new trigonometric shear deformation theory for bending analysis of functionally graded plates resting on elastic foundations. KSCE J Civil Eng 15(8):1405–1414
58. Ramin A, Reddy JN (2009) Nonlocal third-order shear deformation plate theory with application to bending and vibration of plates. J Sound Vib 326(1–2):277–289
59. Sobhy M (2017) A new Quasi 3D nonlocal plate theory for vibration and buckling of FGM nanoplates. IJAM 9(1):1750008
60. Panyatong M, Chinnaboon B, Chucheepsakul S (2016) Free vibration analysis of FG nanoplates embedded in elastic medium based on second-order shear deformation plate theory and nonlocal elasticity. Compos Struct 41(2):666–686